Applied Mathematical Modelling 145 (2025) 116108

Contents lists available at ScienceDirect

Applied Mathematical Modelling

journal homepage: www.elsevier.com/locate/apm

A reduced model for phase-change problems with radiation using simplified P_N approximations

Youssef Belhamadia [a,*], Mohammed Seaid [b]

[a] American University of Sharjah, Department of Mathematics and Statistics, Sharjah, United Arab Emirates
[b] Department of Engineering, University of Durham, South Road, DH1 3LE, United Kingdom

ARTICLE INFO

Keywords:
Radiative heat transfer
Phase change
Simplified P_N approximations
Finite element method
Solidification and melting problems
Asymptotic analysis

ABSTRACT

Radiative heat transfer in phase-change media is of great interest in many thermal applications in sciences and engineering involving internal melting or solidification. In these problems at high temperature, a mathematical model used to describe the heat transfer and phase change should also include equations accounting for thermal radiation. Using the integro-differential equation for the radiative intensity in these models results in a system of coupled equations for which its numerical solution is computationally very demanding. In the present study, we develop a class of efficient reduced models for phase-change problems accounting for grey thermal radiation. The novelty in these models lies in the fact that effects of thermal radiation are well captured in phase-change materials without solving the computationally demanding radiative transfer equation. The model is derived from the enthalpy formulation and the simplified P_N approximations of spherical harmonics. The integro-differential equation for the full radiative transfer is replaced by a set of differential equations which are independent of the angle variable and easy to solve using conventional computational methods. To solve the coupled equations, we implement a second-order implicit scheme for the time integration and a mixed finite element method for the space discretization. A Newton-based algorithm is also adopted for solving the nonlinear systems resulting from the considered monolithic approach. The performance of the proposed reduced models is analyzed on several test examples for coupled radiative heat transfer and phase-change problems in two and three space dimensions. The results presented in this study demonstrate that the proposed models can accurately predict the temperature distributions and capture the phase-change interfaces in melting and solidification examples, all while maintaining a very low computational cost.

1. Introduction

Phase change in materials is very important in a wide variety of engineering applications such as metal processing, crystal growth and additive manufacturing, among others. Under different thermal conditions, these materials undergo phase change such as melting, freezing, casting, ablation, cryosurgery, and soldering. Phase change problems are also crucial for thermal management in various practical applications. Examples include molten salt reactors [1], thermal energy storage [2,3], continuous casting [4,5] and the cooling of semiconductor chips [6] among others. For high-temperature manufacturing processes, the radiation is expected to greatly

* Corresponding author.
E-mail addresses: ybelhamadia@aus.edu (Y. Belhamadia), m.seaid@durham.ac.uk (M. Seaid).

https://doi.org/10.1016/j.apm.2025.116108
Received 27 December 2024; Received in revised form 12 March 2025; Accepted 18 March 2025

Available online 2 April 2025

influence the thermal features and cannot be neglected, especially in semi-transparent materials where the medium does not only reflect and absorb but it also transmits thermal electromagnetic radiation [7,8]. For most of these applications, the heat exchange at the phase-change interface often plays a crucial role and with the thermal radiation affects the shape and structure of the desired materials. Predicting the impact of radiation in materials during the phase-change process through experiments can be very demanding and laborious. Therefore, mathematical modelling and numerical simulations play a crucial role and they can provide accurate and effective thermal predictions in this class of applications. However, modelling coupled radiation-conduction and phase-change problems presents significant challenges due to the complex interactions of radiation and heat exchange between liquid and solid phases.

From a mathematical point of view, the radiative transfer equations are known to be the most accurate model for precisely representing the transfer of photons in a participating medium [8–10]. These governing equations are of the integro-differential type and are solved for the radiative intensity, which depends on time, angle, and spatial coordinates. However, coupling radiation-conduction with phase change is expected to introduce significant numerical complexity and it requires sophisticated computational techniques. Many numerical solvers, including the discontinuous finite element method [11–13] and the adaptive finite element method [14] have been successfully used for combined radiation-conduction heat transfer in participating media. In addition, while these methods have the advantage of accurately determining effects of radiation on the heat transfer, combining radiation with phase change adds considerable numerical complexity. Using the full radiative model coupled with the phase change model demands advanced computational techniques, especially in there-dimensional simulations. In existing literature, the radiative transfer model has been integrated into both the Stefan problem and enthalpy formulation modelling phase-change energy heat transfer. For instance, it has been applied extensively to investigate effects of internal radiative heat transfer in various engineering and industrial applications [15–18]. Various numerical methods have been employed in the literature to address these challenges including standard methods such as the lattice Boltzmann method [19,20], finite volume method [21,22], finite element method [23], and finite difference method [24] for phase change in semi-transparent materials. It should be stressed that, while using these methods to solve the energy formulation, the radiative transfer equation has been solved using the well-established discrete transfer method [20], the discrete ordinates method [25,22], the spherical harmonics method [26], and the simplified spherical harmonics method [27] among others.

While this literature review is not exhaustive, and despite advancements in scientific computing, implementing the full radiative transfer equation to model thermal radiation in participating media remains complex and computationally demanding, especially for three-dimensional simulations. For cases without phase change, numerous studies have concentrated on developing approximate models, instead of incorporating the full radiative transfer model, that accurately describe important physical phenomena while maintaining reasonable computational costs. Numerous approximate equations are available in the literature including the diffusion-type simplified P_N (SP_N) approximations [28,29]. The main advantage of the SP_N approximations is the use of a set of elliptic equations to model radiation transfer that are independent of the angular direction which can be solved using well-established numerical methods for partial differential equations. For optically thick media, the SP_N approximations have been proven to accurately resolve the radiative heat transfer without relying on the integro-differential equations for modelling thermal radiation in glass manufacturing [30], stationary crystal growth [31] and gas turbines [32] among others. We also refer to [33] for a review on approximate models for radiative transfer. Despite being derived in the asymptotic regime for a large optical thickness of the material, these approximations yield encouraging results even in the optically thin regime without phase change in [32,34,29]. However, approximate models for the full radiative heat transfer equations in the presence of phase change are still in their early stages in the literature. Currently, the full model remains the most commonly employed approach for incorporating radiation in both Stefan and enthalpy formulations of phase change models. Recently, a new discontinuous Galerkin method has been developed in [35] for coupling radiation and phase change problems. The enthalpy formulation was coupled with full radiative heat transfer and this method was employed to analyze solidification problems in a two-dimensional case. In [36], a mathematical model coupling phase change and radiation in a non-grey medium was proposed. Similarly, the enthalpy formulation was coupled with the full radiative transfer model but in a non-grey medium, where the full model is transformed into a series of coupled nonlinear equations to be solved for the averaged radiative intensity. In both of these recent contributions, only two-dimensional numerical simulations were performed, and the discrete-ordinates method was used for the full radiative model, which is computationally expensive, especially in the three-dimensional case. Developing a reduced mathematical model for coupling phase change and radiation is therefore needed.

The aim of the current work is to present a class of novel reduced mathematical models for radiative heat transfer in materials undergoing phase change. The central goal is to replace the integro-differential equations commonly used for modelling radiative transfer with a set of simplified partial differential equations that are angle-independent and easy to solve using the conventional numerical techniques for both two- and three-dimensional simulations. For this purpose, we formulate the coupled model of radiative heat transfer and phase change in a dimensionless form using the integro-differential equation coupled to the enthalpy formulation, and introduce a diffusion scale measuring the optical thickness of the medium. Hence, we perform an asymptotic analysis with respect to this optical scale and derive the proposed reduced models using the simplified P_N approximations with a special emphasis on the SP_1 and SP_3 models. It should be stressed that although the simplified P_N approximations are reported in [37] for heat conduction without phase change, the derivation of the SP_N approximations in conjunction with phase change formulation is novel and investigated here for the first time. The proposed reduced radiation-phase-change models offer an equivalent representation to the full radiative transfer while significantly reducing the computational complexity. To solve the developed radiative phase-change models, we employ a mixed finite element method recently introduced by the authors in [38] for the space discretization of conductive SP_N equations. Particularly, high-order elements are employed for the temperature and phase change solutions, while low-order elements are utilized for the radiative solutions. A second-order implicit scheme is used for the time integration and we implement a Newton algorithm to solve the resulting nonlinear system. To examine the proposed methodology, several test examples are considered in two- and

three-dimensional enclosures. We first compare the numerical results obtained using the proposed reduced models to those obtained using the full radiative transfer model for different optical scales. Then, problems of melting sodium chloride and solidification of aluminium are presented illustrating the effects of radiation on the temperature profile and the position of the liquid-solid interface. The presented results demonstrate that the developed reduced models can significantly decrease the computational costs required to achieve a given level of accuracy when solving radiative heat transfer in phase-change media. This offers a significant advantage for modelling radiative transfer in industrial applications where phase change can pose a significant challenge in terms of the required levels of efficiency and accuracy.

The rest of this paper is organized as follows: In section 2, we formulate the equations used to model radiative heat transfer in absorbing and emitting media under phase change. This section begins with the presentation of the dimensional form of the governing equations for coupled full radiative heat transfer and phase change. Then, by introducing a set of reference variables, the equations are reformulated in a dimensionless form. The proposed reduced models for radiative heat transfer in phase change media are presented in section 3 where we conduct an asymptotic analysis of the radiative transfer equation and consider a semi-phase-field approach for the energy equation. In section 4, we discuss the computational techniques used for the numerical solution of the proposed radiation-phase-change models. This section includes the formulation of a fully implicit method for the time integration, a mixed finite element method for the space discretization, and the implementation of the solver for the fully coupled problem. Section 5 is devoted to examine the numerical performance of the developed reduced models through melting and solidification examples. Our approach is demonstrated to enjoy the expected efficiency as well as accuracy. Concluding remarks are summarized in section 6.

2. Equations for radiative heat transfer in phase-change media

In this section we present the governing equations for phase-change problems with radiation using the well-established Stefan and enthalpy formulations. We also reformulate the equations in a dimensionless form and introduce the semi-phase field formulation used in the present study to derive the reduced models.

2.1. Stefan and enthalpy formulations

Assume a geometrical domain $\Omega \subset \mathbb{R}^d$ ($d = 2$ or 3) with the boundary $\partial\Omega$. We consider the medium inside the domain as grey, emitting, absorbing, and scattering the thermal radiation. In the presence of phase change, the radiation model should be combined with the classical Stefan problem that describes the evolution of the interface of a material undergoing a phase change, see [16]. Hence, the heat conduction in the medium Ω, consisting of solid phase $\Omega_s(t)$, liquid phase $\Omega_l(t)$, and the interface $\Gamma(t)$ between them, is described by the following Stefan equations

$$\begin{cases} \rho_s c_s \dfrac{\partial T}{\partial t} - \nabla\cdot(\boldsymbol{K}_s \nabla T) &= -\kappa_s \left(4\pi B(T, n_s) - \displaystyle\int_{\mathbb{S}^2} \psi(\boldsymbol{x}, \boldsymbol{s}) d\boldsymbol{s} \right), & (\boldsymbol{x}, t) \in \Omega_s(t) \times [0, t_f], \\ \rho_l c_l \dfrac{\partial T}{\partial t} - \nabla\cdot(\boldsymbol{K}_l \nabla T) &= -\kappa_l \left(4\pi B(T, n_l) - \displaystyle\int_{\mathbb{S}^2} \psi(\boldsymbol{x}, \boldsymbol{s}) d\boldsymbol{s} \right), & (\boldsymbol{x}, t) \in \Omega_l(t) \times [0, t_f], \\ T(\boldsymbol{x}, t) &= T_f(\boldsymbol{x}, t), & (\boldsymbol{x}, t) \in \Gamma(t) \times [0, t_f], \\ \psi(\boldsymbol{x}, t) &= B(T_f, n), & (\boldsymbol{x}, t) \in \Gamma(t) \times [0, t_f], \\ \left(\boldsymbol{K}_s \boldsymbol{\nabla} T \right) \cdot \boldsymbol{n}_s - (\boldsymbol{K}_l \boldsymbol{\nabla} T) \cdot \boldsymbol{n}_l &= \rho_l L V_\Gamma, & (\boldsymbol{x}, t) \in \Gamma(t) \times [0, t_f], \end{cases} \tag{1}$$

where ρ_k is the density, c_k the specific heat capacity, $\boldsymbol{K}_k$ the thermal conductivity, and κ_k the absorption coefficient, with the subscript $k = l$ or s referring to the liquid or solid phase, respectively. Here, L is the latent heat of fusion, $\mathbb{S}^2$ denotes the unit sphere, $T_f(\boldsymbol{x}, t)$ is the fusion temperature, V_Γ in the interface velocity, $\boldsymbol{n}_s$ and $\boldsymbol{n}_l$ are the exterior unit normal vector to the solid and liquid interface, respectively. In (1), $\psi(\boldsymbol{x}, \boldsymbol{s})$ is the radiative intensity at the space point $\boldsymbol{x}$ along the direction $\boldsymbol{s}$ and is obtained by solving the radiative transfer equations

$$\begin{cases} \boldsymbol{s}\cdot\nabla\psi + \left(\kappa_s + \sigma_s\right)\psi &= \dfrac{\sigma_s}{4\pi} \displaystyle\int_{\mathbb{S}^2} \psi(\boldsymbol{x}, \boldsymbol{s}) d\boldsymbol{s} + \kappa_s B\left(T, n_s\right), & (\boldsymbol{x}, \boldsymbol{s}) \in \Omega_s(t) \times \mathbb{S}^2, \\ \boldsymbol{s}\cdot\nabla\psi + \left(\kappa_l + \sigma_l\right)\psi &= \dfrac{\sigma_l}{4\pi} \displaystyle\int_{\mathbb{S}^2} \psi(\boldsymbol{x}, \boldsymbol{s}) d\boldsymbol{s} + \kappa_l B\left(T, n_l\right), & (\boldsymbol{x}, \boldsymbol{s}) \in \Omega_l(t) \times \mathbb{S}^2, \end{cases} \tag{2}$$

where σ_k is the scattering coefficient of the phase k, with $k = l$ or s. The material is subject to a given initial temperature distribution

$$T(\boldsymbol{x}, 0) = T_0(\boldsymbol{x}), \qquad \boldsymbol{x} \in \Omega, \tag{3}$$

and on the boundary $\partial\Omega$, the heat flux $\boldsymbol{K}\boldsymbol{n}(\hat{\boldsymbol{x}}) \cdot \nabla T$ is defined by a heat convection and diffuse surface radiation as

$$\begin{cases} \boldsymbol{K}_s \boldsymbol{n}(\hat{\boldsymbol{x}}) \cdot \nabla T + \hbar_s (T - T_b) &= \alpha_s \pi \Big(B(T_b, n_b) - B(T, n_s) \Big), & (\hat{\boldsymbol{x}}, t) \in \partial\Omega_s \cap \partial\Omega \times [0, t_f], \\ \boldsymbol{K}_l \boldsymbol{n}(\hat{\boldsymbol{x}}) \cdot \nabla T + \hbar_l (T - T_b) &= \alpha_l \pi \Big(B(T_b, n_b) - B(T, n_l) \Big), & (\hat{\boldsymbol{x}}, t) \in \partial\Omega_l \cap \partial\Omega \times [0, t_f], \end{cases} \tag{4}$$

where $\hbar_k$ is the convective heat transfer coefficient of the phase k, α_k the emissivity coefficient, $T_b(\hat{\boldsymbol{x}}, t)$ is a given temperature of the surrounding, $\boldsymbol{n}(\hat{\boldsymbol{x}})$ denotes the outward normal at $\hat{\boldsymbol{x}}$ with respect to $\partial\Omega$ and $B(T, n_n)$ is the radiative intensity of the black-body radiation given by the Planck function

$$B(T, n_k) = n_k^2 a_R T^4, \tag{5}$$

where n_k is the refractive index of the material k and a_R is the Boltzmann constant [9]. In practice, the radiative transfer equation is equipped with reflective boundary conditions and for completeness, the boundary conditions for the radiative intensity ψ are described in Appendix A.

One of the main difficulties in solving the coupled equations (1)-(2) lies on the fact that the interface $\Gamma(t)$ between the two phases and its velocity V_Γ are not known a priori and they also evolve within the time. To overcome this drawback, an alternative approach is considered for the entire computational domain $\Omega = \Omega_s \cup \Omega_l \cup \Gamma(t)$, known as the enthalpy formulation, see [36]:

$$\begin{cases} \dfrac{\partial H}{\partial t} - \nabla \cdot \Big(\boldsymbol{K}(T) \nabla T \Big) &= -\kappa \left(4\pi B(T, n) - \displaystyle\int_{\mathbb{S}^2} \psi(\boldsymbol{x}, \boldsymbol{s}) d\boldsymbol{s} \right), & (\boldsymbol{x}, t) \in \Omega \times [0, t_f], \\ \boldsymbol{s} \cdot \nabla \psi + \Big(\kappa + \sigma \Big) \psi &= \dfrac{\sigma}{4\pi} \displaystyle\int_{\mathbb{S}^2} \psi(\boldsymbol{x}, \boldsymbol{s}) d\boldsymbol{s} + \kappa B(T, n), & (\boldsymbol{x}, \boldsymbol{s}) \in \Omega \times \mathbb{S}^2, \end{cases} \tag{6}$$

where the enthalpy H is defined by

$$H = \begin{cases} \rho_s c_s T, & \text{if} \quad T < T_f, \\ \rho_l L + \rho_s c_s T_f + \rho_l c_l (T - T_f), & \text{if} \quad T > T_f, \end{cases}$$

the absorption coefficient κ, the scattering coefficient σ, and the refractive index n are defined by

$$\kappa = \begin{cases} \kappa_s, & \text{if} \quad T < T_f, \\ \kappa_l, & \text{if} \quad T > T_f, \end{cases} \qquad \sigma = \begin{cases} \sigma_s, & \text{if} \quad T < T_f, \\ \sigma_l, & \text{if} \quad T > T_f, \end{cases} \qquad n = \begin{cases} n_s, & \text{if} \quad T < T_f, \\ n_l, & \text{if} \quad T > T_f. \end{cases}$$

It should be stressed that based on the analysis reported in [39], the system (6) is equivalent to the problem (1) and it preserves the key properties such that the conditions at the interface are straightforwardly satisfied. Furthermore, system (6) for the enthalpy formulation coupled with the full radiative heat transfer model has been widely used in the literature as the main model for studying effects of thermal radiation in solidification and melting phase change problems, see for instance [17,20,21,35]. In the following sections, we will derive a class of reduced models by simplifying the system (6) into a system that captures effects of internal radiation in grey media during the phase change, while reducing the computational complexity to enhance efficiency for practical applications.

2.2. Semi-phase field formulation

The phase-field approach is widely employed for solving interface problems as an alternative approach to the enthalpy formulation, particularly in solidification and melting applications [40]. In this method, a phase change variable is introduced as a solution to a parabolic-type partial differential equation to determine the evolution of the liquid-solid interface. In the present work, we consider a semi-phase-field approach as an intermediate formulation between the enthalpy and phase-field formulations, we refer to [41,42] for more details. In this approach, the phase change variable is determined by an algebraic equation instead of the parabolic equation. This technique is used for solidification and melting problems where the temperature at the interface is determined by the fusion temperature rather than a term proportional to the sum of interface temperature, curvature, and surface tension. Thus in this study, we introduce the following decomposition

$$H = H_1 + \rho_l L \phi, \tag{7}$$

where H_1 is now a continuous function defined by

$$H_1 = \begin{cases} \rho_s c_s T, & \text{in} \ \ \Omega_s, \\ \rho_s c_s T_f + \rho_l c_l (T - T_f), & \text{in} \ \ \Omega_l, \end{cases} \qquad \text{and} \qquad \phi = \begin{cases} 0, & \text{in} \ \ \Omega_s, \\ 1, & \text{in} \ \ \Omega_l. \end{cases}$$

Hence, replacing the equation (7) in the system (6), a new formulation is obtained which is also equivalent to the classical Stefan problem as

$$\begin{cases} \delta(\phi)\dfrac{\partial T}{\partial t} + \rho L \dfrac{\partial \phi}{\partial t} - \nabla\cdot(\boldsymbol{K}(\phi)\nabla T) &= -\kappa(\phi)\left(4\pi B(T,n) - \displaystyle\int_{\mathbb{S}^2} \psi(\boldsymbol{x},\boldsymbol{s})d\boldsymbol{s}\right), & (\boldsymbol{x},t)\in\Omega\times[0,t_f], \\ \boldsymbol{s}\cdot\nabla\psi + \Big(\kappa(\phi)+\sigma(\phi)\Big)\psi &= \dfrac{\sigma(\phi)}{4\pi}\displaystyle\int_{\mathbb{S}^2}\psi(\boldsymbol{x},\boldsymbol{s})d\boldsymbol{s} + \kappa(\phi)B(T,n), & (\boldsymbol{x},\boldsymbol{s})\in\Omega\times\mathbb{S}^2, \end{cases}$$

where

$$\delta(\phi) = \rho_s c_s + \phi\left(\rho_l c_l - \rho_s c_s\right), \qquad \boldsymbol{K}_c(\phi) = \boldsymbol{K}_s + \phi\left(\boldsymbol{K}_l - \boldsymbol{K}_s\right),$$
$$\kappa(\phi) = \kappa_s + \phi\left(\kappa_l - \kappa_s\right), \qquad \sigma(\phi) = \sigma_s + \phi\left(\sigma_l - \sigma_s\right), \qquad n(\phi) = n_s + \phi\left(n_l - n_s\right).$$

Notice that in practical thermal applications, the phase change occurs in a small temperature range $[T_f-\tau, T_f+\tau]$, with τ is a fixed small parameter. Therefore, the phase-change variable ϕ can be regularized using a function $F_\tau(T)$ defined by

$$\phi := F_\tau(T) = \frac{1}{2} - \frac{1}{2}\tanh\left(\frac{T_f - T}{\tau}\right).$$

Thus, the coupled full radiative and phase-change model considered in this study is formulated as

$$\begin{cases} \delta(T)\dfrac{\partial T}{\partial t} + \rho L \dfrac{\partial F_\tau(T)}{\partial t} - \nabla\cdot(\boldsymbol{K}(T)\nabla T) &= -\kappa(T)\left(4\pi B(T,n) - \displaystyle\int_{\mathbb{S}^2} \psi(\boldsymbol{x},\boldsymbol{s})d\boldsymbol{s}\right), & (\boldsymbol{x},t)\in\Omega\times[0,t_f], \\ \boldsymbol{s}\cdot\nabla\psi + \Big(\kappa(T)+\sigma(T)\Big)\psi &= \dfrac{\sigma_\phi}{4\pi}\displaystyle\int_{\mathbb{S}^2}\psi(\boldsymbol{x},\boldsymbol{s})d\boldsymbol{s} + \kappa(T)B(T,n), & (\boldsymbol{x},\boldsymbol{s})\in\Omega\times\mathbb{S}^2, \end{cases} \tag{8}$$

equipped with the initial condition (3) and the following boundary conditions

$$\begin{cases} \boldsymbol{K}(T)\boldsymbol{n}(\hat{\boldsymbol{x}})\cdot\nabla T + \hbar(T-T_b) &= \alpha\pi\Big(B(T_b,n_b) - B(T,n)\Big), & (\hat{\boldsymbol{x}},t)\in\partial\Omega\times[0,t_f], \\ \psi(\hat{\boldsymbol{x}},\boldsymbol{s}) &= \varrho(\boldsymbol{n}\cdot\boldsymbol{s})\psi(\hat{\boldsymbol{x}},\boldsymbol{s}') + \Big(1-\varrho(\boldsymbol{n}\cdot\boldsymbol{s})\Big)B(T_b,n_b), & (\hat{\boldsymbol{x}},\boldsymbol{s})\in\partial\Omega^-\times\mathbb{S}^2. \end{cases} \tag{9}$$

ϱ_k is the reflectivity coefficient as defined in Appendix A. Since it is convenient to solve the problem using non-dimensional quantities, a dimensionless form of the proposed model (8)-(9) can also be obtained by defining the following dimensionless quantities

$$\boldsymbol{x}^* = \frac{\boldsymbol{x}}{x_{\text{ref}}}, \qquad t^* = \frac{t}{t_{\text{ref}}}, \qquad \kappa^* = \frac{\kappa_\phi}{\kappa_{\text{ref}}+\sigma_{\text{ref}}}, \qquad \sigma^* = \frac{\sigma_\phi}{\kappa_{\text{ref}}+\sigma_{\text{ref}}}, \qquad \hbar^* = \frac{\hbar}{h_{\text{ref}}},$$
$$T^* = \frac{T}{T_{\text{ref}}}, \qquad \psi^* = \frac{\psi}{I_{\text{ref}}},$$

where the subscript ref corresponds to reference quantities. We also impose the relations

$$t_{\text{ref}} = \frac{\rho_{\text{ref}}\, c_{\text{ref}}\, x_{\text{ref}}^2}{K_{\text{ref}}}, \qquad K_{\text{ref}} = \frac{I_{\text{ref}}}{\left(\kappa_{\text{ref}}+\sigma_{\text{ref}}\right)T_{\text{ref}}}, \qquad \hbar_{\text{ref}} = \frac{I_{\text{ref}}}{T_{\text{ref}}}.$$

Hence, the dimensionless form of the system (8), referred to throughout the paper as the PC-RT model, is given by

$$\begin{cases} \delta^*(T^*)\dfrac{\partial T^*}{\partial t} + \dfrac{1}{\text{Ste}}\dfrac{\partial F_\tau(T^*)}{\partial t} - \nabla\cdot\left(\boldsymbol{K}^*(T^*)\nabla T^*\right) &= -\dfrac{1}{\varepsilon^2}\kappa^*(T^*)\left(4\pi B^*(T^*,n) - \displaystyle\int_{\mathbb{S}^2}\psi^*(\boldsymbol{x}^*,\boldsymbol{s})d\boldsymbol{s}\right), & (\boldsymbol{x}^*,\boldsymbol{s})\in\Omega\times\mathbb{S}^2, \\ \varepsilon\,\boldsymbol{s}\cdot\nabla\psi^* + \left(\kappa^*(T^*)+\sigma^*(T^*)\right)\psi^* &= \dfrac{\sigma^*(T^*)}{4\pi}\displaystyle\int_{\mathbb{S}^2}\psi^*(\boldsymbol{x}^*,\boldsymbol{s})d\boldsymbol{s} + \kappa^* B^*(T^*,n), & (\boldsymbol{x}^*,\boldsymbol{s})\in\Omega\times\mathbb{S}^2, \end{cases} \tag{10}$$

subjected to the following boundary and initial conditions

$$\begin{cases} \varepsilon\,\boldsymbol{K}^*(T^*)\boldsymbol{n}(\hat{\boldsymbol{x}})\cdot\nabla T^* + \hbar^*(T^*-T_b^*) &= \alpha\pi\Big(B^*(T_b^*,n_b) - B^*(T^*,n)\Big), & (\hat{\boldsymbol{x}}^*,t^*)\in\partial\Omega, \\ \psi^*(\hat{\boldsymbol{x}}^*,\boldsymbol{s}) &= \varrho(\boldsymbol{n}\cdot\boldsymbol{s})\psi^*(\hat{\boldsymbol{x}}^*,\boldsymbol{s}') + \Big(1-\varrho(\boldsymbol{n}\cdot\boldsymbol{s})\Big)B^*(T_b^*,n_b), & (\hat{\boldsymbol{x}}^*,\boldsymbol{s})\in\partial\Omega^-\times\mathbb{S}^2, \\ T^*(\boldsymbol{x}^*,0) &= T_0^*(\boldsymbol{x}^*), & \boldsymbol{x}^*\in\Omega, \end{cases} \tag{11}$$

where the dimensionless Planck function $B^*(T^*,n)$ is given by

$$B^*(T^*,n)=\frac{n^2 a_R T_{\rm ref}^4 T^{*4}}{I_{\rm ref}}.$$

In (10), Ste is the Stefan number and ε is the optical thickness defined as

$$\mathrm{Ste}=\frac{c_l\,T_{\rm ref}}{L},\qquad \varepsilon=\frac{1}{x_{\rm ref}\left(\kappa_{\rm ref}+\sigma_{\rm ref}\right)},\tag{12}$$

and the transition function and conduction coefficient turn to

$$\delta^*(\phi)=\frac{\rho_s c_s}{\rho_l c_l}+\phi\left(1-\frac{\rho_s c_s}{\rho_l c_l}\right),\qquad \boldsymbol{K}^*(\phi)=\frac{\boldsymbol{K}_s}{K_{\rm ref}}+\phi\left(\frac{\boldsymbol{K}_l}{K_{\rm ref}}-\frac{\boldsymbol{K}_s}{K_{\rm ref}}\right).$$

In what follows, we omit the superscript $*$ from the above equations for ease in the notation. Note that when the absorption coefficient $\kappa^*=0$, the heat phase-change and the radiative transfer equations in (10)-(11) become decoupled and physically no radiation is accounted for in the temperature distribution leading to the following phase-change model with no radiation, referred to throughout the paper as the PC-NoR model.

$$\begin{cases}\delta(T)\dfrac{\partial T}{\partial t}+\dfrac{1}{\mathrm{Ste}}\dfrac{\partial F_\tau(T)}{\partial t}-\nabla\cdot(\boldsymbol{K}(T)\nabla T) &=& 0, & (\boldsymbol{x},t)\in\Omega\times[0,t_f]\\ \boldsymbol{K}(T)\boldsymbol{n}(\hat{\boldsymbol{x}})\cdot\nabla T+\hbar(T-T_b) &=& 0, & (\boldsymbol{x},t)\in\partial\Omega\times[0,t_f]\\ T(\boldsymbol{x},0) &=& T_0(\boldsymbol{x}), & \boldsymbol{x}\in\Omega\end{cases}\tag{13}$$

The model (13) has been studied in several contributions in the literature and it has been verified against exact solutions in two- and three-dimensional enclosures [41,42] and validated against experimental data in [43].

3. New reduced radiative phase-change models

The full-radiative-phase change PC-RT model (10)-(11) is computationally complex due to its reliance on integro-differential equations that depend on time, space, and angle coordinates. To reduce this complexity, the approach aims to replace these integro-differential equations with a set of simplified partial differential equations that are angle-independent. This is achieved by extending the simplified $\mathrm{P_N}$ approximations for radiative heat transfer to phase-change problems in participating media as follows: First Let us define the mean radiative intensity φ and the total scattering $\sigma_{\rm Tot}$ as

$$\varphi=\frac{1}{4\pi}\int_{\mathbb{S}^2}\psi(\boldsymbol{x},\boldsymbol{s})d\boldsymbol{s},\qquad \sigma_{\rm Tot}=\kappa(T)+\sigma(T),$$

then, the full radiative phase change model given by (10) can be reformulated as

$$\begin{cases}\delta(T)\dfrac{\partial T}{\partial t}+\dfrac{1}{\mathrm{Ste}}\dfrac{\partial F_\tau(T)}{\partial t}-\nabla\cdot(\boldsymbol{K}(T)\nabla T) &=& -\dfrac{1}{\varepsilon^2}\kappa(T)\Big(4\pi B(T,n)-\varphi\Big), & (\boldsymbol{x},t)\in\Omega\times[0,t_f],\\ S &=& \dfrac{\sigma}{\sigma_{\rm Tot}}\varphi+\dfrac{\kappa(T)}{\sigma_{\rm Tot}}B(T,n), & \boldsymbol{x}\in\Omega,\end{cases}\tag{14}$$

where

$$S=\left(1+\frac{\varepsilon}{\sigma_{\rm Tot}}\boldsymbol{s}\cdot\nabla\right)\psi.\tag{15}$$

Then, we formally invert the transport operator in (15) using the Neumann series as follows

$$\begin{aligned}\psi&=\left(1+\frac{\varepsilon}{\sigma_{\rm Tot}}\boldsymbol{s}\cdot\nabla\right)^{-1}S,\\ &\approx\left(1-\frac{\varepsilon}{\sigma_{\rm Tot}}\boldsymbol{s}\cdot\nabla+\frac{\varepsilon^2}{\sigma_{\rm Tot}^2}(\boldsymbol{s}\cdot\nabla)^2-\frac{\varepsilon^3}{\sigma_{\rm Tot}^3}(\boldsymbol{s}\cdot\nabla)^3+\frac{\varepsilon^4}{\sigma_{\rm Tot}^4}(\boldsymbol{s}\cdot\nabla)^4+\dots\right)S.\end{aligned}\tag{16}$$

Integrating the expansion (16) with respect to $\boldsymbol{s}$ over all directions in the unit sphere $\mathbb{S}^2$ and using the well-established relation [37]

$$\int_{\mathbb{S}^2}(\boldsymbol{s}\cdot\nabla)^m d\boldsymbol{s}=\Big(1+(-1)^m\Big)\frac{2\pi}{m+1}\nabla^m,\qquad m=1,2,\dots,$$

we obtain the formal asymptotic equation for φ as

$$\varphi=\frac{1}{4\pi}\int_{\mathbb{S}^2}\psi(\boldsymbol{x},\boldsymbol{s})d\boldsymbol{s}=\left(1+\frac{\varepsilon^2}{3\sigma_{\rm Tot}}\nabla^2+\frac{\varepsilon^4}{5\sigma_{\rm Tot}^4}\nabla^4+\frac{\varepsilon^6}{7\sigma_{\rm Tot}^6}\nabla^6+\dots\right)S+\mathcal{O}\left(\varepsilon^8\right),\tag{17}$$

where the notation $\mathcal{O}$ refers to the order of approximations. Hence,

$$
\begin{aligned}
S &= \left(1+\frac{\varepsilon^2}{3\sigma_{\rm Tot}}\nabla^2+\frac{\varepsilon^4}{5\sigma_{\rm Tot}^4}\nabla^4+\frac{\varepsilon^6}{7\sigma_{\rm Tot}^6}\nabla^6+\ldots\right)^{-1}\varphi+\mathcal{O}(\varepsilon^8)\\
&=\left(1-\left(\frac{\varepsilon^2}{3\sigma_{\rm Tot}}\nabla^2+\frac{\varepsilon^4}{5\sigma_{\rm Tot}^4}\nabla^4+\frac{\varepsilon^6}{7\sigma_{\rm Tot}^6}\nabla^6\right)+\left(\frac{\varepsilon^2}{3\sigma_{\rm Tot}}\nabla^2+\frac{\varepsilon^4}{5\sigma_{\rm Tot}^4}\nabla^4+\frac{\varepsilon^6}{7\sigma_{\rm Tot}^6}\nabla^6\right)^2-\right.\\
&\quad\left.\left(\frac{\varepsilon^2}{3\sigma_{\rm Tot}}\nabla^2+\frac{\varepsilon^4}{5\sigma_{\rm Tot}^4}\nabla^4+\frac{\varepsilon^6}{7\sigma_{\rm Tot}^6}\nabla^6\right)^3\cdots\right)^{-1}\varphi+\mathcal{O}(\varepsilon^8).
\end{aligned}
$$

This yields to the formal asymptotic equation for the mean intensity φ as

$$
S=\left(1-\frac{\varepsilon^2}{3\sigma_{\rm Tot}^2}\nabla^2-\frac{4\varepsilon^4}{45\sigma_{\rm Tot}^4}\nabla^4-\frac{44\varepsilon^6}{94\sigma_{\rm Tot}^6}\nabla^6\right)\varphi+\mathcal{O}(\varepsilon^8). \tag{18}
$$

Thus, the full radiative phase-change PC-RT model can be rewritten in an angle-independent form as

$$
\left\{\begin{array}{rcll}
\delta(T)\dfrac{\partial T}{\partial t}+\dfrac{1}{\rm Ste}\dfrac{\partial F_\tau(T)}{\partial t}-\nabla\cdot(\boldsymbol{K}(T)\nabla T) &=& -\dfrac{1}{\varepsilon^2}\kappa(T)\,(4\pi B(T,n)-\varphi), & (\boldsymbol{x},t)\in\Omega\times[0,t_f],\\
\left(1-\dfrac{\varepsilon^2}{3\sigma_{\rm Tot}^2}\nabla^2-\dfrac{4\varepsilon^4}{45\sigma_{\rm Tot}^4}\nabla^4-\dfrac{44\varepsilon^6}{94\sigma_{\rm Tot}^6}\nabla^6\right)\varphi+\mathcal{O}(\varepsilon^8) &=& \dfrac{\sigma}{\sigma_{\rm Tot}}\varphi+\dfrac{\kappa(T)}{\sigma_{\rm Tot}}B(T,n), & \boldsymbol{x}\in\Omega.
\end{array}\right. \tag{19}
$$

By neglecting terms of the leading order $\mathcal{O}(\varepsilon^2)$, $\mathcal{O}(\varepsilon^4)$, $\mathcal{O}(\varepsilon^6)$ or $\mathcal{O}(\varepsilon^8)$ one obtains the PC-SP$_0$, PC-SP$_1$, PC-SP$_2$ or PC-SP$_3$ models, respectively. Note that higher order approximations can also be derived following the same formalism. In this study, we consider only the PC-SP$_1$ and PC-SP$_3$ models, and our computational techniques can be straightforwardly extended to other approximations. To derive the boundary conditions for the SP$_{\rm N}$ approximations, variational principles similar to those used in the well-established Marshak conditions for P$_{\rm N}$ approximations in [44,37] are used. In this section, we present the proposed reduced PC-SP$_1$ and PC-SP$_3$ models as follows:

By neglecting terms of the leading order $\mathcal{O}(\varepsilon^4)$ in (18), the source S can be approximated as

$$
S=\varphi-\frac{\varepsilon^2}{3\sigma_{\rm Tot}^2}\nabla^2\varphi+\mathcal{O}(\varepsilon^4),
$$

and therefore the system (19) yields the following reduced system

$$
\left\{\begin{array}{rcll}
\delta(T)\dfrac{\partial T}{\partial t}+\dfrac{1}{\rm Ste}\dfrac{\partial F_\tau(T)}{\partial t}-\nabla\cdot(\boldsymbol{K}(T)\nabla T) &=& -\dfrac{1}{\varepsilon^2}4\pi\kappa(T)\Big(B(T,n)-\varphi\Big), & (\boldsymbol{x},t)\in\Omega\times[0,t_f],\\
-\dfrac{\varepsilon^2}{3\,(\kappa+\sigma)}\nabla^2\varphi+\kappa\varphi &=& 4\pi\kappa B(T,n), & \boldsymbol{x}\in\Omega,
\end{array}\right. \tag{20}
$$

equipped with the initial condition (3) and the following boundary conditions

$$
\left\{\begin{array}{rcll}
\varepsilon\boldsymbol{K}(T)\boldsymbol{n}(\hat{\boldsymbol{x}})\cdot\nabla T+\hbar(T-T_b) &=& \alpha\pi\Big(B(T_b,n_b)-B(T,n)\Big), & (\hat{\boldsymbol{x}},t)\in\partial\Omega\times[0,t_f],\\
\left(\dfrac{2\varepsilon\zeta}{3\,(\kappa+\sigma)}\right)\boldsymbol{n}(\hat{\boldsymbol{x}})\cdot\nabla\varphi &=& 4\pi B(T_b,n_b), & \hat{\boldsymbol{x}}\in\partial\Omega
\end{array}\right. \tag{21}
$$

For the second reduced model for coupling radiation-phase-change problems, we neglect terms of the leading order $\mathcal{O}(\varepsilon^8)$ in (18) to obtain an approximation of S as

$$
S=\left(1-\frac{\varepsilon^2}{3\,(\kappa+\sigma)^2}\nabla^2-\frac{4\varepsilon^4}{45\,(\kappa+\sigma)^4}\nabla^4-\frac{44\varepsilon^6}{94\,(\kappa+\sigma)^6}\nabla^6\right)\varphi+\mathcal{O}(\varepsilon^8),
$$

and thus the system (19) yields the following reduced system

$$
\left\{\begin{array}{rcll}
\delta(T)\dfrac{\partial T}{\partial t}+\dfrac{1}{\rm Ste}\dfrac{\partial F_\tau(T)}{\partial t}-\nabla\cdot(\boldsymbol{K}(T)\nabla T) &=& -\dfrac{1}{\varepsilon^2}4\pi\kappa(T)\left(B(T,n)-\dfrac{\gamma_2\varphi_1-\gamma_1\varphi_2}{\gamma_2-\gamma_1}\right), & (\boldsymbol{x},t)\in\Omega\times[0,t_f],\\
-\dfrac{\varepsilon^2\mu_1^2}{3\,(\kappa+\sigma)}\nabla^2\varphi_1+\kappa\varphi_1 &=& 4\pi\kappa B(T,n), & \boldsymbol{x}\in\Omega,\\
-\dfrac{\varepsilon^2\mu_2^2}{3\,(\kappa+\sigma)}\nabla^2\varphi_2+\kappa\varphi_2 &=& 4\pi\kappa B(T,n), & \boldsymbol{x}\in\Omega,
\end{array}\right. \tag{22}
$$

equipped with the initial condition (3) and the following boundary conditions

$$\begin{cases} \varepsilon \boldsymbol{K}(T)\boldsymbol{n}(\hat{\boldsymbol{x}})\cdot\nabla T + \hbar(T-T_b) &= \alpha\pi\Big(B(T_b,n_b)-B(T,n)\Big), & (\hat{\boldsymbol{x}},t)\in\partial\Omega\times[0,t_f],\\ \varpi_1\varphi_1 + \dfrac{\varepsilon}{\kappa+\sigma}\boldsymbol{n}(\hat{\boldsymbol{x}})\cdot\nabla\varphi_1 &= -\beta_2\varphi_2+\eta_1 B(T_b,n_b), & \hat{\boldsymbol{x}}\in\partial\Omega,\\ \varpi_2\varphi_2 + \dfrac{\varepsilon}{\kappa+\sigma}\boldsymbol{n}(\hat{\boldsymbol{x}})\cdot\nabla\varphi_2 &= -\beta_1\varphi_1+\eta_2 B(T_b,n_b), & \hat{\boldsymbol{x}}\in\partial\Omega. \end{cases} \tag{23}$$

In the sequel, the new reduced systems (20)-(21) and (22)-(23) are referred to as PC-SP$_1$ and PC-SP$_3$ models, respectively. It should be noted that the parameters ζ, μ_i, ϖ_i, β_i, η_i, and γ_i (with $i=1,2$) appearing in (21), (22) and (23) are derived using asymptotic and variational analyses, see [37] for detailed derivation of these parameters. For completeness, the required formulae for calculating these parameters are summarized in Appendix B. From the mathematical asymptotic used to derive the simplified P$_N$ approximations, it is clear that the smaller the diffusion scale ε is, the better approximation is achieved in these models and at the leading order when the diffusion scale goes to zero, one exactly recovers the full radiative transfer model. However, from a physical perspective and in the computational radiative transfer, the diffusion scale is defined as the inverse of the product of domain thickness and total scattering coefficient as given by equation (12). In practical applications with known material and thermal properties, the diffusion scale is calculated using (12) and it is not necessarily close to zero.

4. Numerical methods and solution procedure

Numerical solutions of the coupled PC-SP$_1$ model (20)-(21) and the coupled PC-SP$_3$ model (22)-(23) can be achieved using any computational method designed for solving partial differential equations of elliptic-parabolic types. For example, finite elements methods are well established for its flexibility in dealing with complex geometries and have been proven to be suitable for solving the SP$_N$ approximations of radiative heat transfer using unified variational formulations, see for example [30,45,46,14]. In these unified finite element methods, the same finite element space is used for the spatial discretization of the temperature solution and the radiative mean intensity. Recently, a mixed finite element method has been proposed in [38] to solve the SP$_N$ approximations of radiative heat transfer for which different finite element spaces are employed for discretization of the temperature solution and radiative mean intensity. In the present study, this mixed finite element method is adopted to solve the coupled PC-SP$_N$ models using the quadratic $\mathbb{P}_2$ elements for the temperature solution and the linear $\mathbb{P}_1$ elements for the radiative solutions. For the time integration, we use the second-order implicit backward differentiation formula (BDF2) also known as the Gear scheme [47]. In this section we only formulate the method for the coupled PC-SP$_3$ model (22)-(23) and its formulation for the coupled PC-SP$_1$ model (20)-(21) can be carried out in a similar manner. Hence, the time interval $[0,t_f]$ is divided into N subintervals $[t_k,t_{k+1}]$ with uniform length $\Delta t = t_{k+1}-t_n$ for $k=0,1,\ldots,N$ and we use the notation $w^k = w(\boldsymbol{x},t_k)$ to denote the value of a generic function w at time t_k. For the spatial discretization, we discretize the domain Ω into a finite set of conforming elements $\mathcal{K}_j$ ($j=1,2,\ldots N_e$) with N_e is the total number of elements and the computational domain $\Omega_h\subseteq\Omega$ is the combination of all these finite elements. We also define the conforming finite element spaces V_h and W_h as

$$V_h = \Big\{ T_h\in C^0(\overline{\Omega}):\quad T_h\Big|_{\mathcal{K}}\in\mathbb{P}_2(\mathcal{K}),\quad \forall\,\mathcal{K}\in\Omega_h\Big\},$$
$$W_h = \Big\{ \psi_h\in C^0(\overline{\Omega}):\quad \psi_h\Big|_{\mathcal{K}}\in\mathbb{P}_1(\mathcal{K}),\quad \forall\,\mathcal{K}\in\Omega_h\Big\},$$

where $\mathbb{P}_2(\mathcal{K})$ and $\mathbb{P}_1(\mathcal{K})$ are polynomial spaces defined in the finite element $\mathcal{K}$ of degree 2 and 1, respectively. Therefore, using (ψ_1,ψ_2,ψ_3) as test functions, the weak formulation of the coupled PC-SP$_3$ model (22)-(23) reads as: Find $\left(T^{k+1},\varphi_1^{k+1},\varphi_2^{k+1}\right)\in V_h\times W_h\times W_h$, such that

$$\begin{aligned} &\int_\Omega \delta(T^{k+1})\frac{3T^{k+1}-4T^k+T^{k-1}}{2\Delta t}\psi_1 d\boldsymbol{x} + \frac{1}{\mathrm{Ste}}\int_\Omega \frac{3F_\tau(T^{k+1})-4F_\tau(T^k)+F_\tau(T^{k-1})}{2\Delta t}\psi_1 d\boldsymbol{x} + \\ &\int_\Omega \cdot\left(\boldsymbol{K}(T^{k+1})\nabla T^{k+1}\right)\cdot\nabla\psi_1 d\boldsymbol{x} = \frac{\kappa}{\varepsilon^2}\int_\Omega\left(\frac{\gamma_2\varphi_1^{k+1}-\gamma_1\varphi_2^{k+1}}{\gamma_2-\gamma_1}-4\pi B\left(T^{k+1},n\right)\right)\psi_1\,d\boldsymbol{x} + \\ &\frac{\hbar}{\varepsilon}\oint_{\partial\Omega}\left(T_b-T^{k+1}\right)\psi_1\,d\boldsymbol{x} + \frac{\alpha\pi}{\varepsilon}\oint_{\partial\Omega}\Big(B(T_b,n_b)-B\left(T^{k+1},n\right)\Big)\psi_1\,d\boldsymbol{x}, \end{aligned} \tag{24}$$

$$\begin{aligned} &\frac{\varepsilon^2\mu_1^2}{3(\kappa+\sigma)}\int_\Omega\nabla\varphi_1^{k+1}\cdot\nabla\psi_2\,d\boldsymbol{x} + \kappa\int_\Omega\varphi_1^{k+1}\psi_2\,d\boldsymbol{x} = 4\pi\kappa\int_\Omega B\left(T^{k+1},n\right)\psi_2\,d\boldsymbol{x} + \\ &\frac{\varepsilon\mu_1^2}{3}\oint_{\partial\Omega}\Big(\eta_1 B(T_b,n_b)-\beta_2\varphi_2^{k+1}-\varpi_1\varphi_1^{k+1}\Big)\psi_2\,d\boldsymbol{x}, \end{aligned}$$

$$\frac{\varepsilon^2\mu_2^2}{3(\kappa+\sigma)}\int_\Omega \nabla\varphi_2^{k+1}\cdot\nabla\psi_3\,d\boldsymbol{x}+\kappa\int_\Omega \varphi_2^{k+1}\psi_3\,d\boldsymbol{x}=4\pi\kappa\int_\Omega B\left(T^{k+1},n\right)\psi_3\,d\boldsymbol{x}+$$
$$\frac{\varepsilon\mu_2^2}{3}\oint_{\partial\Omega}\left(\eta_2 B(T_b,n_n)-\beta_1\varphi_1^{k+1}-\varpi_2\varphi_2^{k+1}\right)\psi_3\,d\boldsymbol{x}.$$

Next, a finite element discretization of the weak form (24) is carried out for assembling the associated mass and stiffness matrices. This step is straightforward and for brevity in the presentation it is omitted here. Note that the equations (24) are nonlinear and fully coupled to be solved monolithically for the triplet solution $\left(T^{k+1},\varphi_1^{k+1},\varphi_2^{k+1}\right)$. For all numerical results reported in this study, a Newton-based method is employed to solve these nonlinear systems at each timestep and the resulting linear systems are solved using a GMRES-SOR algorithm from the PETSc[1] library, see for example [48,49]. Here, the convergence of the Newton iterations is achieved when the residual norm is less than 10^{-6}. In our simulations, it has been found that three to five iterations were sufficient to achieve this required convergence.

5. Numerical results and examples

We present numerical results for three examples of phase-change problems with radiation to demonstrate the accuracy and efficiency of the proposed simplified models. The main advantage of the proposed models in this study is their ability to provide numerical solutions for the coupled radiative heat transfer and phase-change problems in a simplified manner without relying on the highly demanding solutions of the integro-differential equations for the radiative transfer. To illustrate the reliability and accuracy of the proposed models, numerical results are presented for two- and three-dimensional problems. First, we conduct a verification study of the asymptotic analysis to compare numerical results obtained using the proposed coupled PC-SP_1 model and the coupled PC-SP_3 model to those obtained using the coupled full radiative transfer phase-change (PC-RT) model at different optical regimes. In the second example, we examine the performance of the proposed PC-SP_3 model for a melting problem of sodium chloride in two- and three-dimensional enclosures. Our final example considers a problem of solidification of aluminium in a three-dimensional domain to assess the capability of the proposed models for solving phase-change problems with radiation in complex geometries. All the computations reported in this section were performed on a Dell Precision 7920 Tower with 20C Dual Intel Xeon Gold 6148 2.4 GHz processor and 64 GB 2666 MHz DDR4 Memory. Notice that all the considered methods are tested for problems with known analytical solutions and the expected convergence orders are obtained, ensuring the correctness and robustness of our computational techniques.

5.1. Verification results for the asymptotic analysis

We first verify the asymptotic analysis performed to derive the PC-SP_1 and PC-SP_3 models for phase-change problems with radiation. To this end, we compare the temperature distributions of the proposed PC-SP_1 and PC-SP_3 models to those obtained using the full PC-RT model for a benchmark problem widely used in the literature for validating the SP_N approximations for radiative heat transfer with no phase change, see for example [37,30,29,14]. In this example, we use the same problem but we extend it to include phase change in the medium. In particular, we consider a two-dimensional enclosure $\Omega=[0,1]\times[0,1]$ filled with a hot liquid at an initial temperature of $T_0=1500\,\mathrm{K}$. The hot liquid is cooled down from its boundaries using the Robin-type boundary conditions, with a convective heat transfer coefficient of $\hbar=1$ and a boundary temperature of $T_b=300\,\mathrm{K}$. During the cooling process, the hot material undergoes transformation into a solid state at the fusion temperature $T_f=1400\,\mathrm{K}$. We assume a non-scattering medium with the scattering coefficient $\sigma=0$, the absorption coefficient $\kappa=1$, the conduction $\boldsymbol{K}=\mathbf{I}$, with $\mathbf{I}$ is the unity matrix, $\tau=1\,\mathrm{K}$, and the Stefan number set to $\mathrm{Ste}=1$. Here, we solve the equations (20)-(21), (22)-(23), and (10)-(11) for respectively, PC-SP_1, PC-SP_3 and PC-RT models, and we compare the obtained results for the temperature and phase-change solutions for two different values of the optical scale ε. A structured mesh with 200×200 elements with a fixed timestep $\Delta t=10^{-7}$ is used in simulations of the PC-SP_1 and PC-SP_3 models. To solve the radiative transfer equation in PC-RT model, we employ the Diffusion Synthetic Acceleration (DSA) method which uses the diffusion approach to accelerate the source iterations from the computational radiative transfer, see [32,50] for a detailed implementation of the DSA method. The S_8 discrete-ordinate set is used for the angle discretization in (10)-(11) along with a structured uniform mesh of 400×400 gridpoints are used in our computations. Note that these mesh and angle discretizations yield linear systems with 128×10^5 unknowns to be solved at each time step. In Fig. 1, we present snapshots of the temperature T and phase-change variable ϕ obtained using $\varepsilon=1$ at the time $t=5\times10^{-5}$, and those results obtained using $\varepsilon=0.1$ at the final time $t=10^{-5}$ are displayed in Fig. 2. It is clear that for the considered diffusion scales, the results obtained using the proposed PC-SP_1 and PC-SP_3 models exhibit different patterns for $\varepsilon=1$ especially for the phase change solutions, compare the phase-change interfaces in Fig. 1. Decreasing the diffusion scale to $\varepsilon=0.1$ results in a similar pattern for both temperature and phase-change solutions in Fig. 2. This confirms the asymptotic analysis performed to derive the PC-SP_1 and PC-SP_3 models. To further demonstrate this asymptotic analysis, we present in Fig. 3 cross-sections of the temperature and phase-change variable solutions at the main diagonal corresponding to $y=x$ for both considered optical scales $\varepsilon=1$ and $\varepsilon=0.1$. It is evident that the proposed simplified models preserve the thermal radiative structures of the phase change at the optical regimes considered. The boundary features of the temperature

[1] http://www.mcs.anl.gov/petsc/.

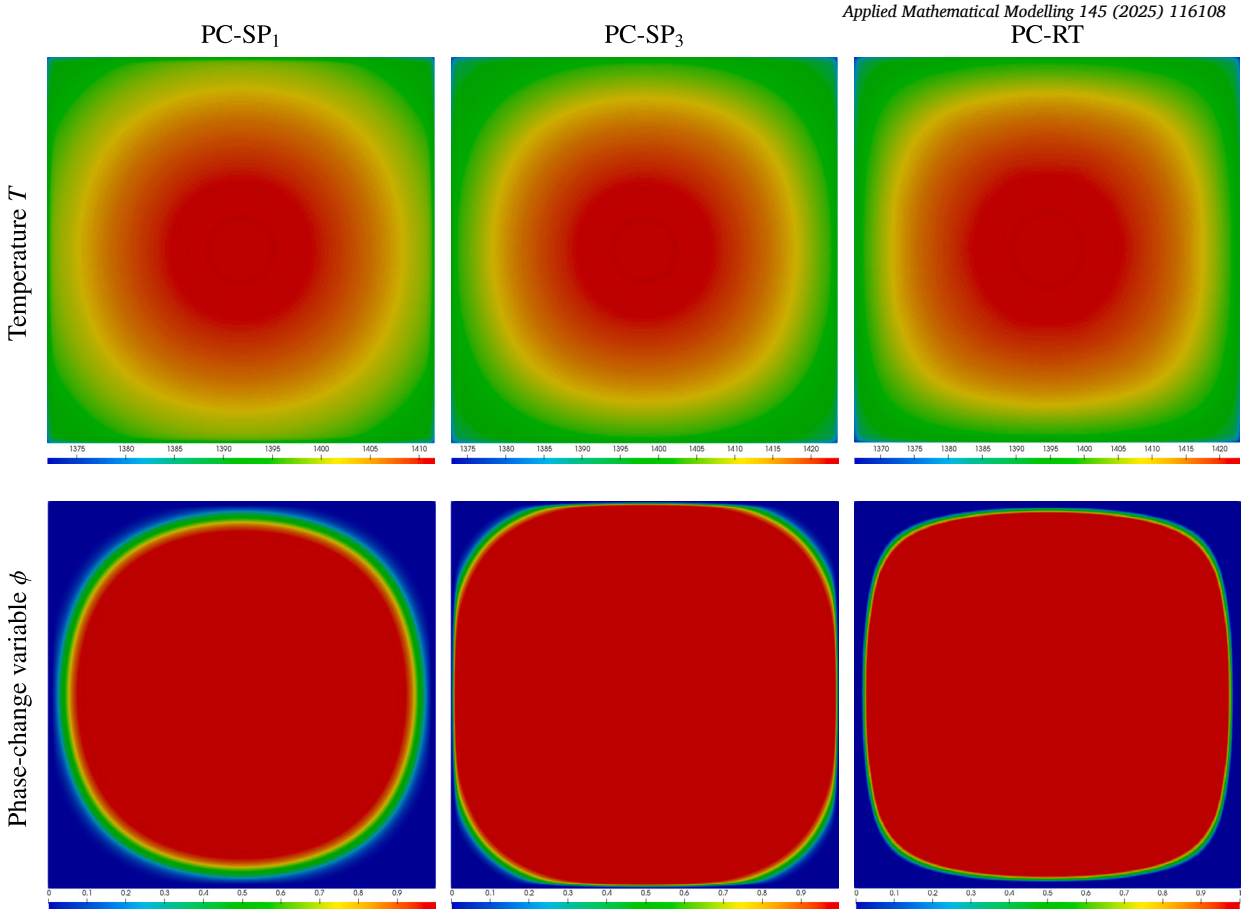

Fig. 1. Results for the temperature (first row) and the phase-change variable ϕ (second row) obtained for the two-dimensional verification problem using the PC-SP$_1$ model (first column), the PC-SP$_3$ model (second column), and the PC-RT model (third column) with $\varepsilon = 1$ at time $t = 5 \times 10^{-5}$.

Table 1
Errors in the temperature T and the phase-change variable ϕ obtained using PC-SP$_1$ and PC-SP$_3$ models for the two-dimensional verification problem with $\varepsilon = 0.1$ at time $t = 10^{-5}$.

	$\varepsilon = 0.1$			
	Temperature T		Phase ϕ	
	PC-SP$_1$	PC-SP$_3$	PC-SP$_1$	PC-SP$_3$
L^1-error	0.0105	0.0054	0.0791	0.0573
L^2-error	0.0125	0.0055	0.2670	0.2214

are also captured by our finite element method and they compare well with those obtained using the DSA solver for the radiative transfer equation. These results clearly emphasize that solutions obtained using the full PC-RT and PC-SP$_3$ models closely coincide. At the asymptotic limit $\varepsilon = 0.1$, the PC-SP$_1$ and PC-SP$_3$ models deliver temperature and phase-change variable solutions similar to those obtained using the full PC-RT model. Therefore, one may conclude that the proposed PC-SP$_3$ model performs very well for this coupled radiative heat transfer and phase-change problem. It is important to note that the results of the PC-SP$_3$ model align well with the full radiative model results even with a large ε, whereas the PC-SP$_1$ model is preferable when ε is small. To further quantify the errors between the results obtained using the full radiative transfer model and those obtained using the proposed PC-SP$_1$ and PC-SP$_3$ models for this example, we present in Table 1 the computed relative L^1-error and L^2-error for the case with $\varepsilon = 0.1$ at time $t = 10^{-5}$. These results clearly show that the solutions obtained with the proposed PC-SP$_3$ model and the full PC-RT model nearly coincide. Furthermore, the calculated errors are smaller using PC-SP$_3$ model compared to PC-SP$_1$ model, which also confirms the asymptotic analysis performed to derive the PC-SP$_1$ and PC-SP$_3$ models.

In terms of the computational cost, both PC-SP$_1$ and PC-SP$_3$ models demonstrate rapid convergence compared to the full PC-RT model at the considered optical scales. It is evident that, for this test example, the PC-SP$_1$ and PC-SP$_3$ models asymptotically resolve

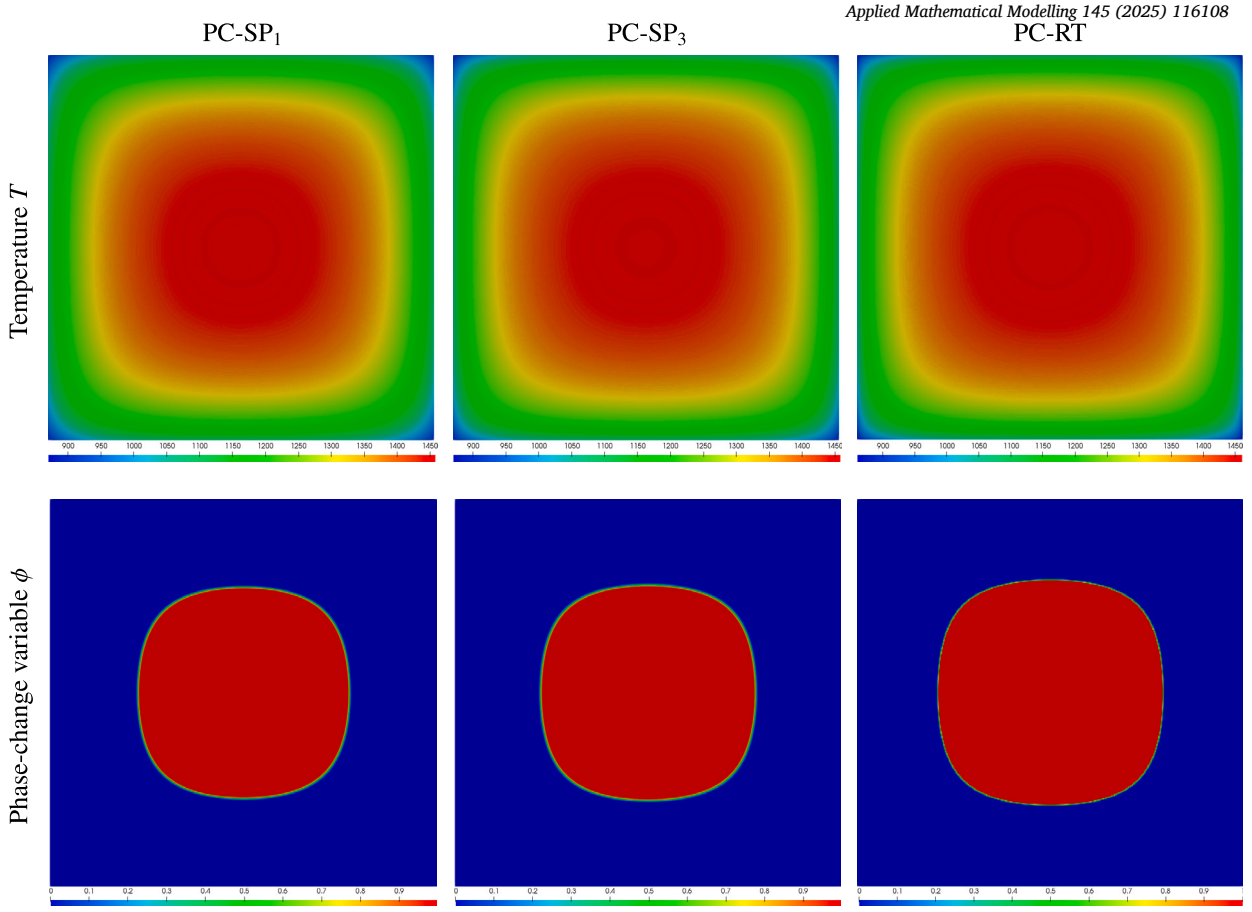

Fig. 2. Results for the temperature (first row) and the phase-change variable ϕ (second row) obtained for the two-dimensional verification problem using the PC-SP_1 model (first column), the PC-SP_3 model (second column), and the PC-RT model (third column) with $\varepsilon = 0.1$ at time $t = 10^{-5}$.

the coupled radiative heat transfer and phase-change equations as the DSA method does, but with very less computational effort referring to the CPU times. Particularly, solving the PC-SP_3 model exhibits fast convergence with a CPU time approximately 11 times lower compared to the full PC-RT model for a similar accuracy. Similarly, solving the PC-SP_1 model demonstrates fast convergence with a CPU time approximately 15 times lower compared to the full PC-RT model for a similar level of accuracy. These findings underscore the effectiveness of the proposed PC-SP_N models in accurately capturing radiation effects in optically thick media. This is achieved without the need for solving the integro-differential equations typically employed in the literature for radiative transfer but instead, the models solve one or two additional elliptic equations for the PC-SP_1 model or the PC-SP_3 model, respectively. It is worth mentioning that for the optical scale $\varepsilon = 1$, the numerical solution is found to be sensitive to the choice of the mesh size. This is well-known in the literature when there is no phase change, see for example [30]. We have also experienced this behaviour in our case, where the material undergoes a phase change. This can be seen in Fig. 4, where we present cross-sections of the temperature using the PC-SP_3 model along the main diagonal corresponding to $y = x$ using four different structured meshes with 25×25, 50×50, 100×100 and 200×200 elements at two different times. We can clearly see that while the oscillations can be present when coarse meshes are used, the boundary features of the temperature are well captured on finer meshes. This mesh refinement study also demonstrates the numerical convergence of the methodology adopted in the current work. Notice that we have also performed this study for the PC-SP_1 model, where we observed similar numerical behaviour and to avoid repetition, we present only the results for the PC-SP_3 model.

Next, we consider a three-dimensional version of this coupled radiative heat transfer and phase-change problem to show the asymptotic analysis in the proposed PC-SP_1 and PC-SP_3 models. Hence, we solve the equations (20)-(21) and (22)-(23) in the unit cube $\Omega = [0,1] \times [0,1] \times [0,1]$ using the same parameters as in the previous two-dimensional case. A structured mesh with 3072000 tetrahedral elements is used in our simulation and the time-step is fixed to $\Delta t = 10^{-7}$. Fig. 5 depicts the obtained results for the temperature and phase-change variable using the PC-SP_3 model with $\varepsilon = 0.1$ at three different times namely $t = 10^{-6}$, $t = 5 \times 10^{-6}$ and $t = 10^{-5}$. For a better visualization, only parts of the computational domain are illustrated in this figure. It is clear that as the time progresses, the medium becomes cooler due to the heat release through the domain boundaries. The proposed simplified models resolve these expected thermal and phase-change features at low computational cost compared to the full PC-RT model. Notice that for the selected optical scale, results obtained using the PC-SP_1 model are very similar to those obtained using the PC-SP_3 model

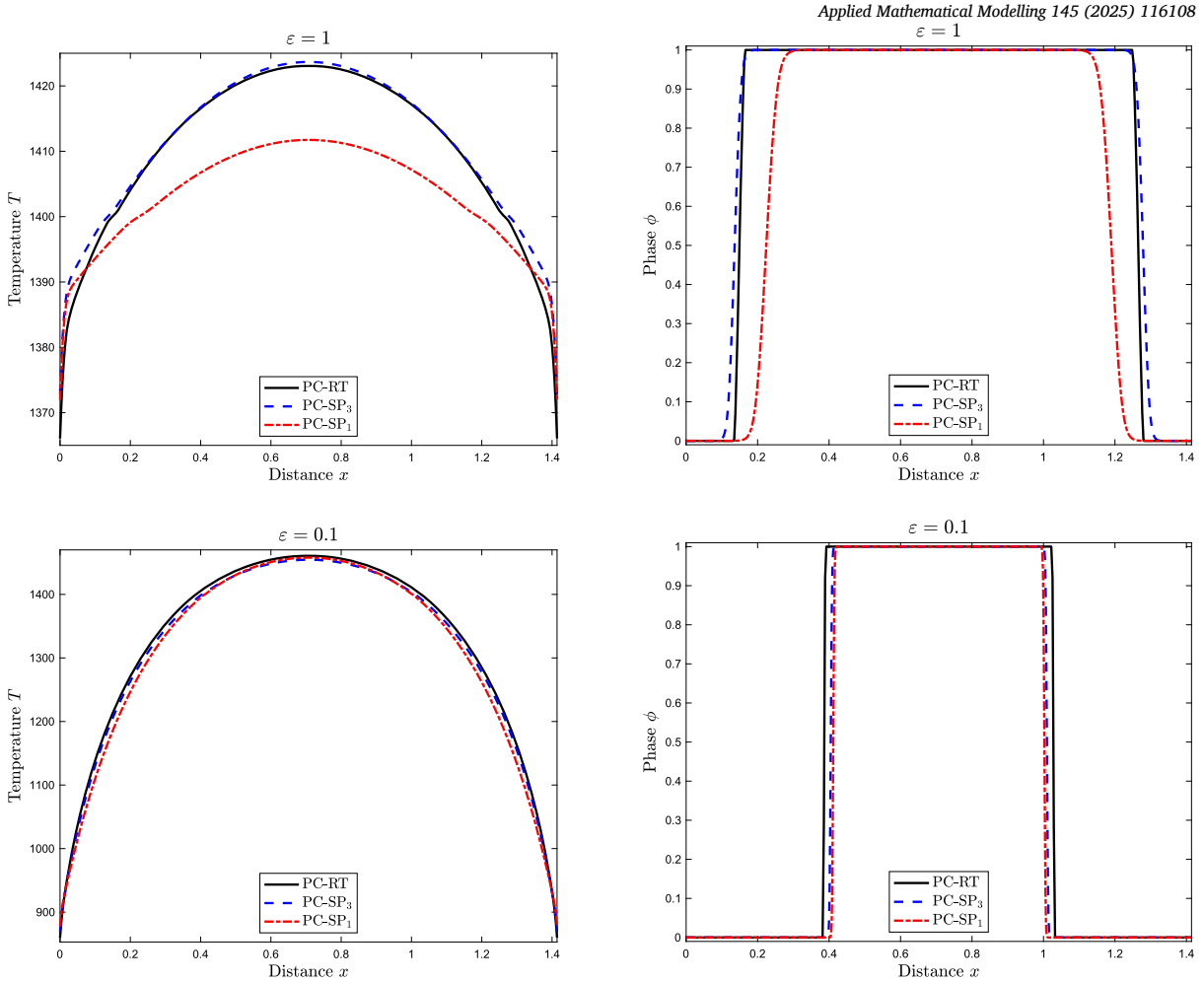

Fig. 3. Cross-sections of the results presented in Fig. 1 and Fig. 2 along the main diagonal $y = x$.

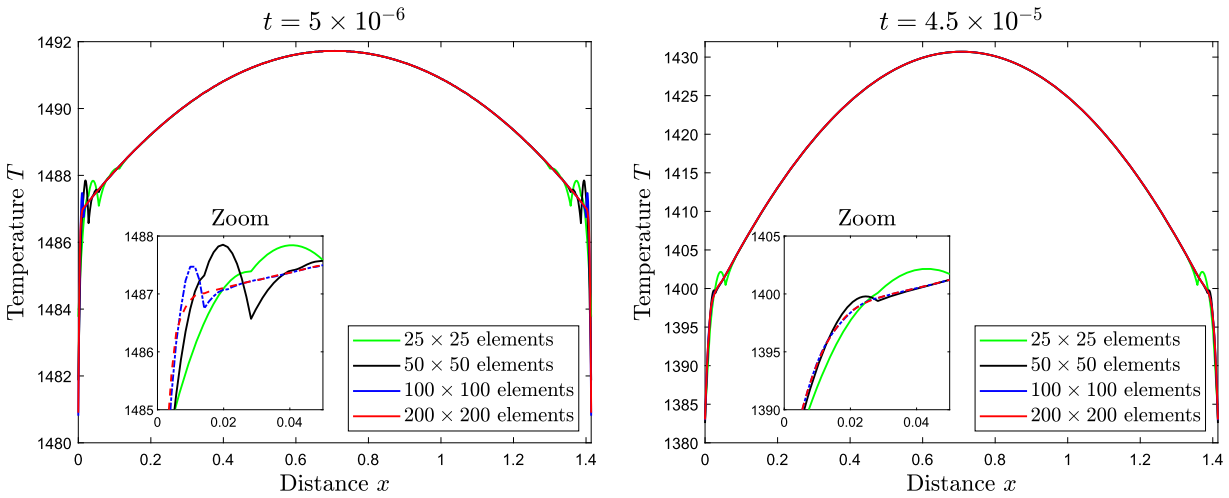

Fig. 4. Cross-sections of the results obtained with the PC-SP$_3$ model for the two-dimensional verification problem along the main diagonal using different meshes at time $t = 5 \times 10^{-6}$ (left plot) and at time $t = 4.5 \times 10^{-5}$ (right plot).

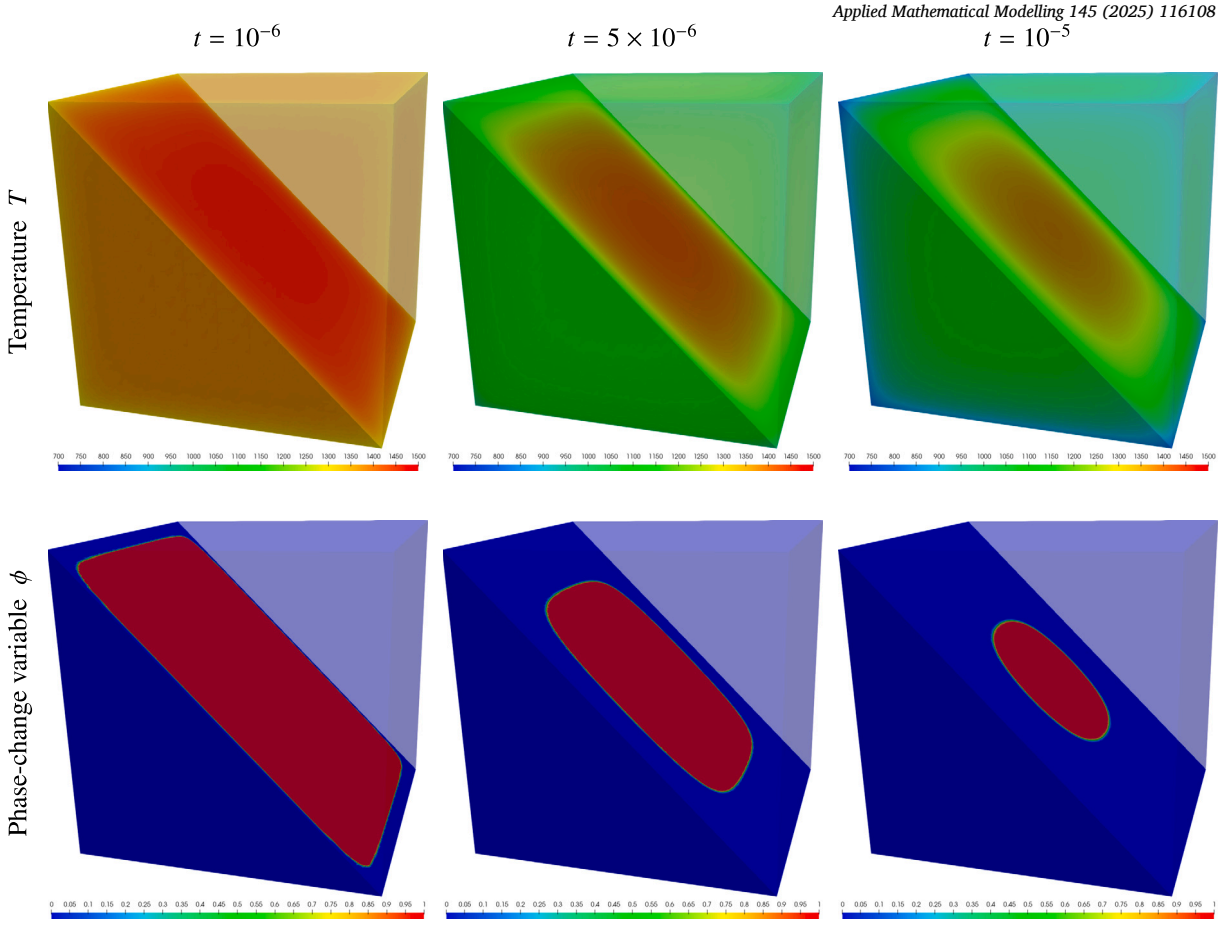

Fig. 5. Results for the temperature (first row) and the phase-change variable ϕ (second row) obtained for the three-dimensional verification problem using the PC-SP$_3$ model with $\varepsilon = 0.1$ at three different times $t = 10^{-6}$ (first column), $t = 5 \times 10^{-6}$ (second column), and t $= 10^{-5}$ (third column).

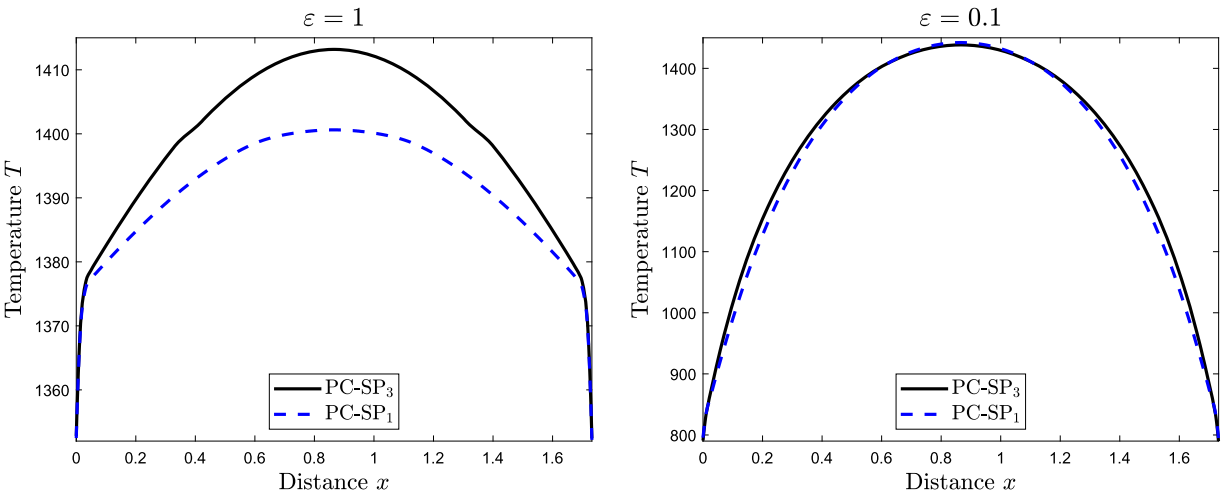

Fig. 6. Cross-sections of the results obtained for the three-dimensional verification problem using the PC-SP$_1$ and PC-SP$_3$ models along the main diagonal at time $t = 5 \times 10^{-5}$ for $\varepsilon = 1$ (left plot) and at time $t = 10^{-5}$ for $\varepsilon = 0.1$ (right plot).

and therefore and are not included here. It should also be noted that we do not include results obtained using the full radiative transfer phase-change model since implementing the DSA method in three dimensions is computationally very demanding and it is not within the scope of this study. To evidence the asymptotic limits for this test example we also present in Fig. 6 cross-sections of

Table 2
Reference parameters used in our simulations for melting problem of sodium chloride.

$\boldsymbol{K}_s = \boldsymbol{K}_l = (-0.269 + 9.07910^{-4}T)\mathbf{I}\ \left(\mathrm{W\cdot m^{-1}\cdot K^{-1}}\right)$	$k_{\mathrm{ref}} = 0.86\ \left(\mathrm{W\cdot m^{-1}\cdot K^{-1}}\right)$
$c_s = 1662.3 - 0.4218T\ \left(\mathrm{J\cdot kg^{-1}\cdot K}\right)$	$c_{\mathrm{ref}} = 1180\ \left(\mathrm{J\cdot kg^{-1}\cdot K}\right)$
$c_l = 3289.3 - 3.4589T + 0.0014173T^2\ \left(\mathrm{J\cdot kg^{-1}\cdot K}\right)$	$x_{\mathrm{ref}} = 0.05\ \mathrm{(m)}$
$\rho_l = 2168.1 - 0.5663T\ \left(\mathrm{kg\cdot m^{-3}}\right)$	$\rho_{\mathrm{ref}} = 1460\ \left(\mathrm{kg\cdot m^{-3}}\right)$
$\kappa = 10, 40, 80\ \left(\mathrm{m^{-1}}\right)$	$\kappa_{\mathrm{ref}} = \kappa$
$L = 479289\ \left(\mathrm{J\cdot kg^{-1}}\right)$	$T_b = 1150, 1200, 1250\ \mathrm{(K)}$
$a_R = 5.67\times 10^{-8}\ \left(\mathrm{W\cdot m^{-2}\cdot K^4}\right)$	$\sigma_{\mathrm{ref}} = a_R$
$t_{\mathrm{ref}} = 5000\ \mathrm{(s)}$	$\mathrm{Ste} = 0.0025$

the temperature solutions obtained using the PC-SP_1 and PC-SP_3 models with two different diffusion scales $\varepsilon = 1$ and $\varepsilon = 0.1$. As can be clearly seen in this figure, a large discrepancy between the results is detected for $\varepsilon = 1$ but decreasing this scale to $\varepsilon = 0.1$, this discrepancy becomes negligible. Again as in the two-dimensional case, the PC-SP_1 and PC-SP_3 models give similar results at the asymptotic limit when ε is small. Needless to mention that solving the three-dimensional full PC-RT model is very demanding from a computational point of view. However, adopting the proposed PC-SP_N models in optically thick media offers a simplified and cost-effective approach for capturing radiation effects in phase-change problems. This is mainly because the radiative equation in the full PC-RT model requires solving the integro-differential equations, whereas the simplified PC-SP_N models incorporate the radiation effect by only solving a set of additional elliptic equations. Note that based on the results obtained for this example in two and three space dimensions, results obtained using the PC-SP_3 model are more accurate than those obtained using the PC-SP_1 model when compared to the full PC-RT model. Therefore, only results obtained using the PC-SP_3 model are presented for the remaining examples.

5.2. Melting problem of sodium chloride

Phase change materials are considered as effective tools for improving the thermal performance of the solar heating systems and, at high temperatures, thermal radiation can significantly impact this process. Recently, investigations reported in [2] have demonstrated that the thermal radiation accelerates the phase transition and it reduces the melting time in these problems. In [2], a discrete-ordinate method was employed for the radiative heat transfer coupled with the momentum equation and enthalpy porosity formulation in a two-dimensional axisymmetric finned cylinder. Although we do not employ the same set of equations in the present study, we aim to replicate similar melting behaviour using our proposed PC-SP_3 model. In our simulations for this problem, we consider both two- and three-dimensional cases using similar thermal and radiation parameters as in [2]. However, unlike in [2] where the physical properties were considered as independent of temperature except for the density in the momentum equations, in the current work, the physical properties for sodium chloride are considered temperature-dependent as provided in [2] and summarized in Table 2.

In our first run in this problem, we consider a two-dimensional case where the computational domain is a circle with four fins. The circle has a radius of 5 mm, and the fins are 30 mm long with a thickness of 1 mm. The sodium chloride with a high melting temperature of $T_f = 1074\,\mathrm{K}$, is chosen as the phase change material and initially, the material is in the solid state with a temperature of 970 K which is below the melting temperature. The material is then heated from the boundaries by setting the surrounding temperature at $T_b = 1150\,\mathrm{K}$. In our computations, the domain is discretized in an unstructured triangular mesh with around 79000 elements leading to 521624 degrees of freedom (dof) for T, 40211 dof for ϕ_1, and 40211 dof for ϕ_2 and the timestep is set to $\Delta t = 10\,\mathrm{s}$. The obtained results for the temperature and phase-change variable using the PC-NoR model are shown in Fig. 7 at four different times $t = 100\,\mathrm{s}$, $t = 200\,\mathrm{s}$, $t = 250\,\mathrm{s}$, and $t = 300\,\mathrm{s}$. The melting process can clearly be seen in these results as the temperature distributions exhibit high thermal fronts propagating from the domain boundary towards the center as the time evolves. The time evolution of the phase-change interfaces in this figure also follows the temperature distributions as the material is melted. At the time $t = 300\,\mathrm{s}$, only a small area remains solid within the domain center whereas the other parts become liquid. The proposed numerical techniques perform well for this phase-change problem as no spurious oscillations are detected in the obtained results and a full symmetry is captured for both temperature and phase-change solutions.

To examine effects of radiation on the melting process for this problem, we compare numerical simulations obtained with radiation using the PC-SP_3 model at three different optical regimes corresponding to $\varepsilon = 2$, $\varepsilon = 0.5$, and $\varepsilon = 0.25$ to those obtained without radiation by eliminating all source terms in the PC-SP_3 equations leading to the PC-NoR model in (13). For this comparison, we monitor the temperature solution at center of the domain over the first 90 min of the simulation and the computed results are presented in Fig. 8. Under the considered phase-change conditions, it is evident that the inclusion of radiation in the model enhances the melting rates. The melting process is initiated when the variable ϕ is slightly above 0 which occurs at approximately 1 min in the presence of radiation compared to around 22 min when the radiation is not accounted for. A similar conclusion was drawn in [2], where it was noted that the melting occurred around 4 min when considering radiation compared to around 30 min for simulations with no radiation. In addition, it was reported in [2] that the total transition time (*i.e.* the time to reach a liquid fraction corresponding to an interface ϕ of 0.999) depends on the presence of radiation effects in the model under study. For instance, the total transition time in [2] decreased from 92 min with no radiation to 32 min with radiation. In our simulations using the PC-SP_3 model, this total transition time is decreased from 61 min with no radiation to 5.5 min with radiation. It is worth noting that as shown in Fig. 8, the melting process initiates earlier when $\varepsilon = 0.25$ compared to the melting time observed when $\varepsilon = 0.5$. This behaviour has also been observed in the results published in [2]. It should be stressed that, while we have not anticipated replicating the exact melting process

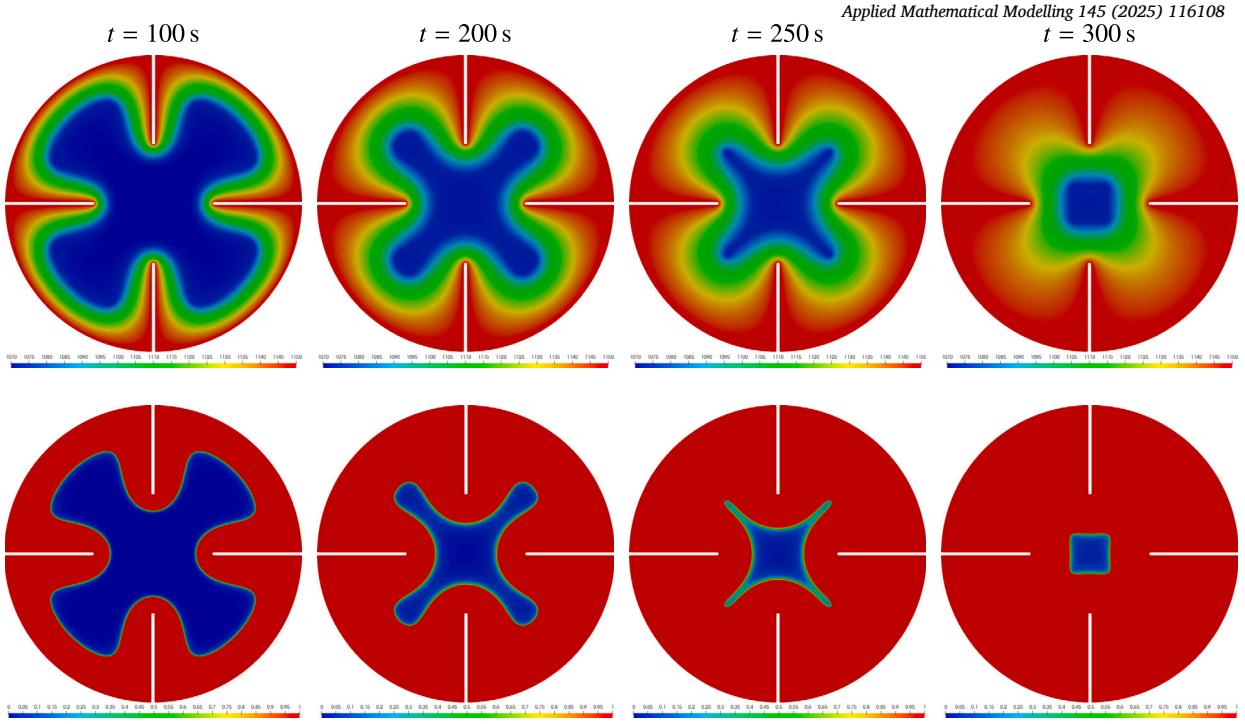

Fig. 7. Results for the temperature (first row) and the phase-change variable ϕ (second row) obtained for the melting problem of sodium chloride in the two-dimensional domain at four different times $t = 100\,\text{s}$, $t = 200\,\text{s}$, $t = 250\,\text{s}$ and $t = 300\,\text{s}$.

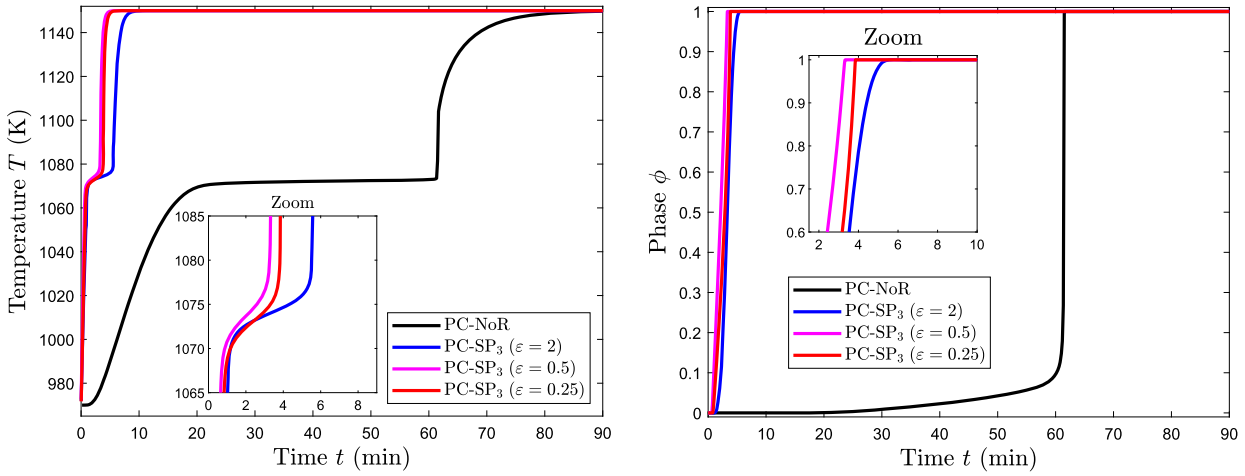

Fig. 8. Time evolution of the temperature (left plot) and the phase-change variable ϕ (right plot) obtained at the domain center for the melting problem of sodium chloride in the two-dimensional domain with and without radiation.

observed in [2] due to the utilization of different sets of equations, our findings revealed similar melting behaviour with and without radiation for this problem. It worth mentioning that there may not be noticeable differences in results obtained using PC-SP_1 model or PC-SP_3 model for small values of the optical thickness, but we have presented our results using the PC-SP_3 model to demonstrate its flexibility, not only in the small optical thickness regime but also in the large ones.

Our next concern with this example is to investigate the impact of radiation on the temperature when the material is subjected to different boundary temperatures. Therefore, we perform simulations for this test example using the PC-SP_3 model with three different ambient temperatures namely, $T_b = 1150\,\text{K}$, $1200\,\text{K}$, and $1250\,\text{K}$. The obtained results for the time evolution of the phase-change variable ϕ for $\varepsilon = 2$ and $\varepsilon = 0.25$ at the center of the domain are illustrated in Fig. 9. These results confirm our expectations and show a faster melting process for simulations with higher boundary temperatures T_b. Again, this underscores the effectiveness of our methodology in modelling the impact of radiative effects on the phase change materials, and all this is achieved without the need for solving the integro-differential equations for radiative heat transfer.

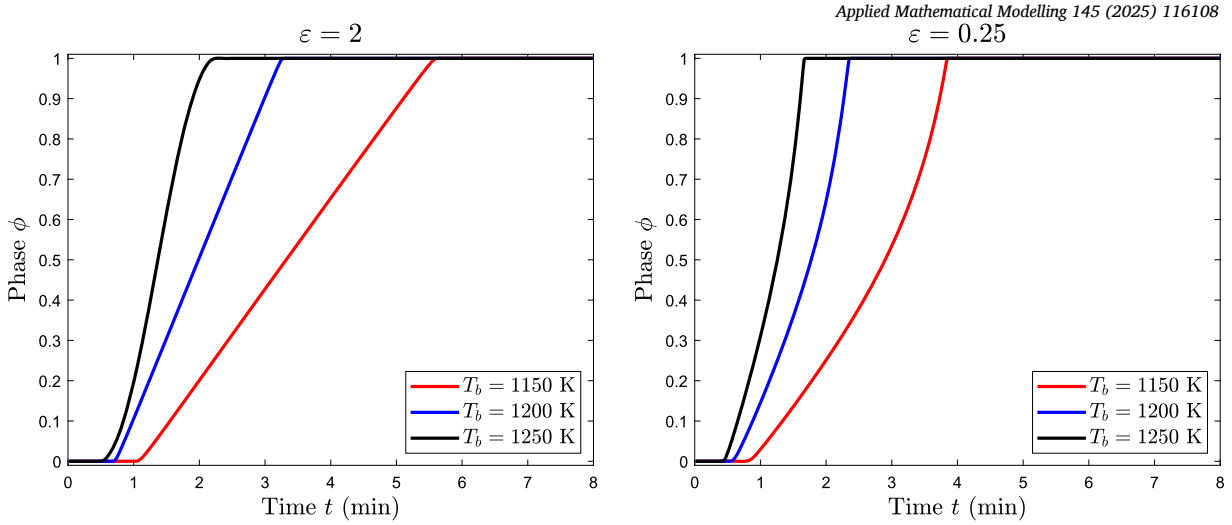

Fig. 9. Time evolution of the phase-change variable ϕ for $\varepsilon = 2$ (left plot) and $\varepsilon = 0.25$ (right plot) obtained at the domain center for the melting problem of sodium chloride in the two-dimensional domain using three different ambient temperatures.

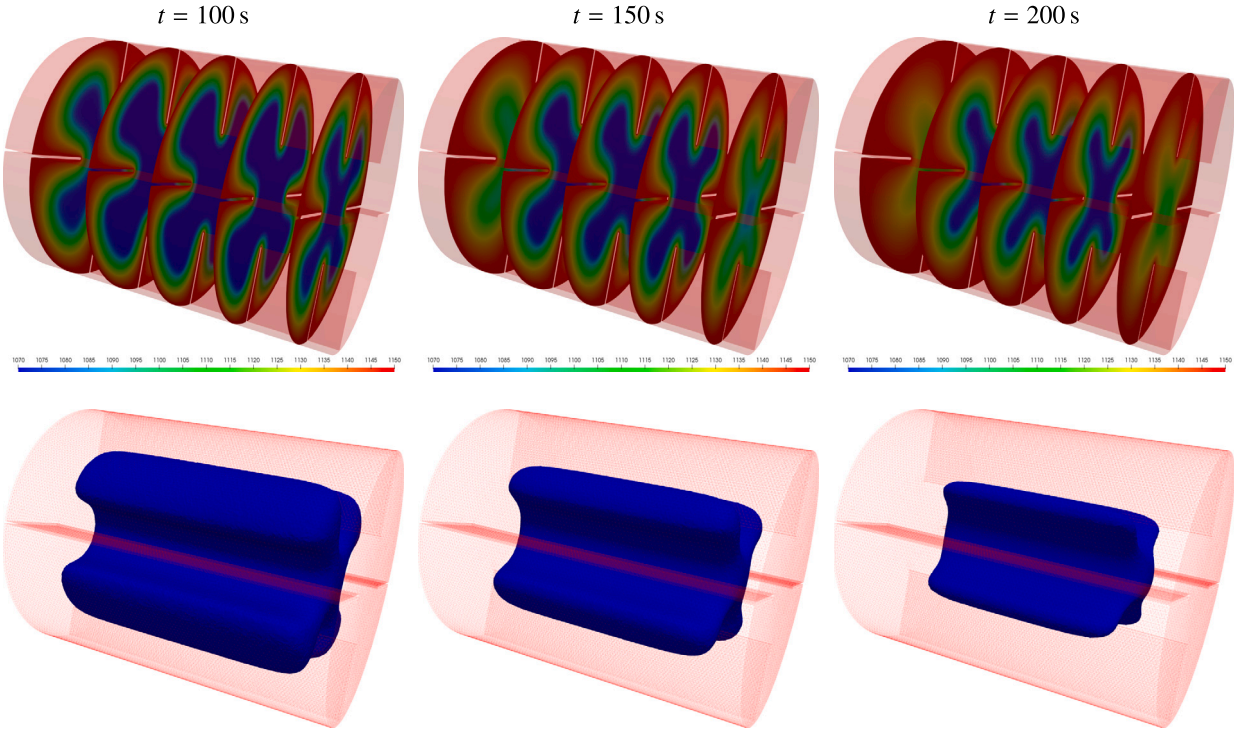

Fig. 10. Results for the temperature (first row) and the phase-change variable ϕ (second row) obtained for the melting problem of sodium chloride in the three-dimensional domain at three different times $t = 100$ s, $t = 150$ s, and 200 s.

Encouraged by these two-dimensional results, we have extended our investigation to the three-dimensional situation of this coupled radiative heat transfer and phase-change problem. Thus, we reconstruct a three-dimensional domain by elongating the previous two-dimensional geometry into a cylinder with a length of 250 mm. We maintained the same physical parameters as in the two-dimensional case and solve both the PC-NoR and PC-SP$_3$ models using an unstructured mesh with around 202800 tetrahedral elements leading to 2838950 dof for T, 373057 dof for ϕ_1, and 373057 dof for ϕ_2. Fig. 10 illustrates the obtained results for the temperature and phase change solutions at three different times $t = 100$ s, $t = 150$ s, and 200 s using the PC-NoR model. As in the two-dimensional simulations, the melting process is clearly observed in these results as the temperature distributions show high thermal fronts propagating from the domain boundaries towards the center as the time progresses. These effects can also be clearly seen in the time evolution of the phase-change interfaces as the melting occurs within the computational domain. The numerical performance of the methodology

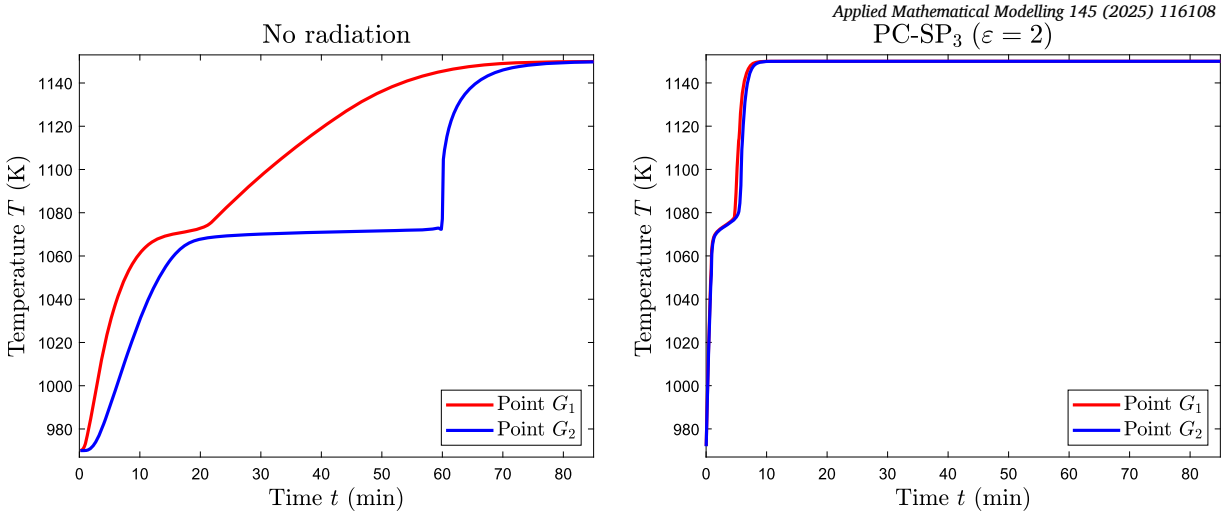

Fig. 11. Time evolution of the temperature obtained at the selected points G_1 and G_2 with no radiation (left plot) and with radiation (right plot) for the melting problem of sodium chloride in the three-dimensional domain.

Table 3
Reference parameters used in our simulations for the solidification problem of aluminium.

$\boldsymbol{K}_s = \boldsymbol{K}_l = 231\mathbf{I}$ $(\mathrm{W}\cdot\mathrm{m}^{-1}\cdot\mathrm{K}^{-1})$	$c_s = c_l = 900$ $(\mathrm{J}\cdot\mathrm{kg}^{-1}\cdot\mathrm{K})$
$\rho_l = 2700$ $(\mathrm{kg}\cdot\mathrm{m}^{-3})$	$L = 396400$ $(\mathrm{J}\cdot\mathrm{kg}^{-1})$
$\kappa = 10$ (m^{-1})	$\sigma = 0$ (m^{-1})
$a_R = 5.67\times 10^{-8}$ $(\mathrm{W}\cdot\mathrm{m}^{-2}\cdot\mathrm{K}^{4})$	$\varepsilon = 0.1$

proposed in this study is also confirmed by this three-dimensional problem. To further assess the impact of radiation on the melting process, we compare numerical results obtained for this problem without radiation using the PC-NoR model to those with radiation using the PC-SP$_3$ model at $\varepsilon = 2$. For comparison, we monitor the computed temperatures at two different points G_1 and G_2 located in the computational domain at $G_1 = (0, 0, 0.25)$ and $G_2 = (0, 0, 1.25)$, respectively. The time evolutions of the temperature at these selected points are depicted in Fig. 11 and the obtained results demonstrate similar melting behaviours to that observed in the two-dimensional case. Hence, we conclude that the radiation significantly accelerates the melting process, and our proposed simplified models effectively incorporate radiation in the phase change materials using only sets of elliptic equations without accounting for the integro-differential equations for radiative heat transfer. It should be pointed out that the presence of radiation yields a sharper liquid-solid interface, which may also affect the numerical method by requiring a smaller time step and a larger value of τ; otherwise, the Newton method may not converge. In particular, the PC-SP$_3$ model may require a smaller time step and a larger value of τ compared to the PC-NoR model. For instance, in our three-dimensional computations, while we used $\Delta t = 10\,\mathrm{s}$ and $\tau = 2\,\mathrm{K}$ when solving the PC-NoR model, $\Delta t = 1\,\mathrm{s}$ and $\tau = 4\,\mathrm{K}$ were needed for the PC-SP$_3$ model.

5.3. Solidification problem of aluminium

Our final example consists of assessing the performance of the proposed PC-SP$_3$ model for a three-dimensional phase-change problem involving solidification of the aluminium. It has been shown in many studies that the radiation affects the temperature profiles in the solidification process of materials, see for instance [23,16,20]. More precisely, it has been reported in this reference that the thermal radiation accelerates the phase transition and thus, affects the liquid-solid interface. This class of problems is also widely used in manufacturing engineering of continuous cast aluminium for which the primary zone in the continuous casting process experiences the highest temperature difference. Furthermore, at this zone the liquid aluminium is continuously poured to the mould and it starts to solidify from the wall boundaries yielding the initial shape of the required aluminium product. As a consequence, the radiation in this zone is expected to significantly impact both the solid-liquid interface and the thermal features in the mould due to the high temperature involved in this process. To demonstrate these effects, we consider a solidification problem in a three-dimensional $\Omega = [0, 1] \times [-0.25, 0.25] \times [0, 1]$ that includes two hollow cylinders of radius 0.1. The enclosure is initially filled with aluminium in its liquid state at a temperature of $T_0 = 1300\,\mathrm{K}$ and the material undergoes solidification starting from the two cylinders kept at fixed boundary temperature of $T_b = 300\,\mathrm{K}$ which is below the freezing temperature of $\Theta_f = 925\,\mathrm{K}$. The other boundaries of the computational domain are also set to the ambient temperature of $T_b = 300\,\mathrm{K}$. Here, the physical properties of aluminium reported in [51] and summarized in Table 3 are used in our simulations. An unstructured mesh with around 2020000 tetrahedral elements leading to 2813149 dof for T, 367699 dof for ϕ_1, and 367699 dof for ϕ_2 is used for the spatial discretization and the timestep is fixed to $\Delta t = 4\,\mathrm{s}$ and based on Table 3, the value of τ is set to $5\,\mathrm{K}$.

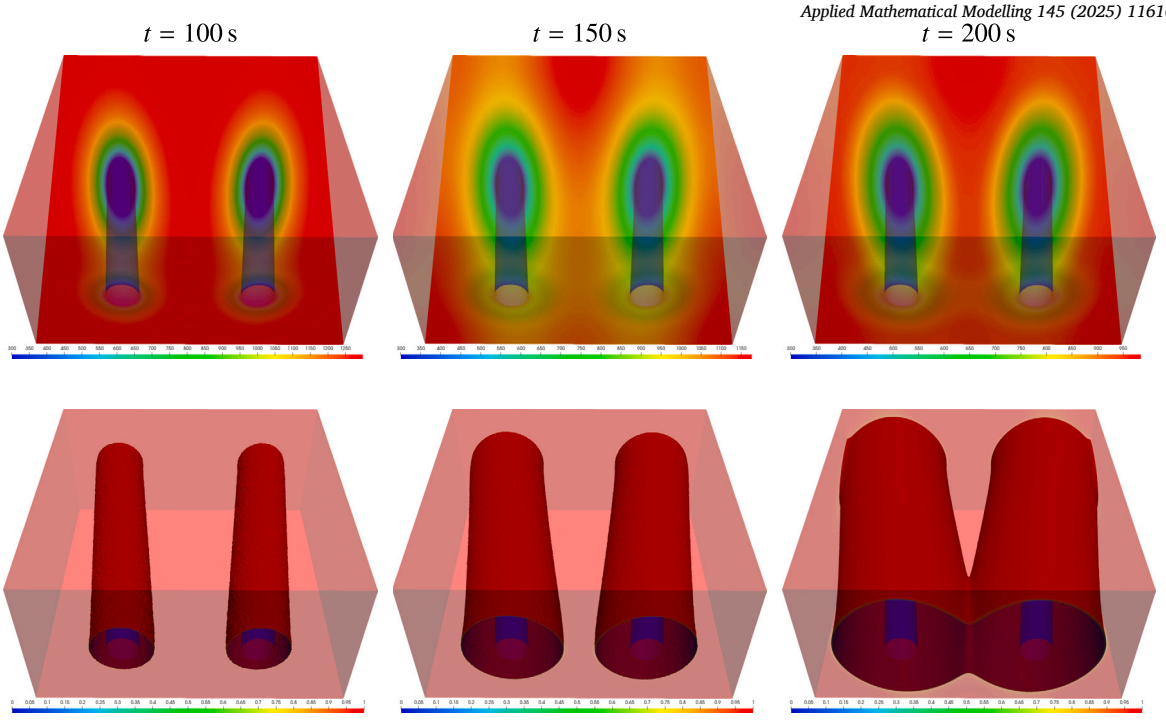

Fig. 12. Results for the temperature (first row) and the phase-change variable ϕ (second row) obtained for the solidification problem of aluminium in the three-dimensional domain at three different times $t = 40\,\text{s}$, $t = 200\,\text{s}$ and $t = 400\,\text{s}$.

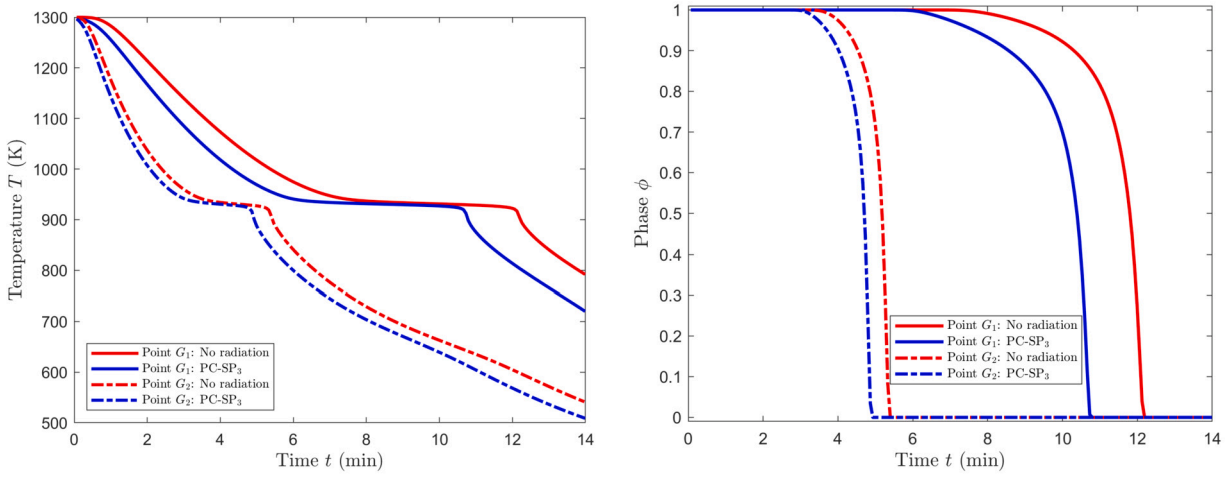

Fig. 13. Time evolution of the temperature (left plot) and the phase-change variable ϕ (right plot) obtained at the selected points G_1 and G_2 with and without radiation for solidification problem of aluminium in the three-dimensional domain.

In Fig. 12 we present the obtained results for the temperature and phase change solutions at three different times $t = 40\,\text{s}$, $t = 200\,\text{s}$ and $t = 400\,\text{s}$ using the PC-NoR model. The solidification process can be clearly observed in these results as the temperature exhibits low thermal fronts propagating within the time from the walls of the two hollow cylinders outwards the surrounding medium. The results obtained for the phase-change interfaces clearly illustrate these thermal patterns as the solidification takes place around the cylinders in the computational domain. To demonstrate the effect of radiation on the thermal behaviour of this phase-change example, we illustrate in Fig. 13 the time evolution of the computed temperature and phase-change interface using both PC-NoR and PC-SP_3 models at two different points G_1 and G_2 located in the computational domain at $G_1 = (0.5, 0, 0)$ and $G_2 = (0.5, 0, 1)$, respectively. It is clear from all these profiles that the inclusion of thermal radiation affects the temperature distribution and it also accelerates the solidification process as previously reported in the literature for this class of solidification problems. This can be clearly detected from the interface positions shown in Fig. 13 since the interface position in the presence of radiation (plotted in blue colour) is more advanced compared to the interface without radiation (plotted in red colour). In summary, for the considered radiation condition,

the radiation noticeably accelerates the solidification procedure, and our proposed simplified PC-SP_3 model successfully includes these radiative effects in the phase change materials by replacing the computationally demanding solver of the integro-differential radiative transfer equations by a robust finite element solution of two additional elliptic equations which asymptotically recover the full radiative solutions for optically thick media. It should also be mentioned that the efficiency of the proposed mixed finite element method is reflected in the reduction in the total number of degrees of freedom and the reduction in the size of associated systems of algebraic equations required to be solved at each time step to update the solution. Finally, we also note that the proposed mixed finite element method is highly attractive for computational heat transfer.

6. Conclusions

A class of highly efficient mathematical models has been proposed in the present study for solving radiative heat transfer in phase-change media. The governing equations for the phase change employ the enthalpy formulation resulting in a single nonlinear equation to be solved for the temperature. Using a diffusion scale to measure the optical thickness of the medium under study, an asymptotic analysis is carried out on the integro-differential equation of radiative transfer to derive the simplified P_N approximations. Coupled to equations of the phase-change, this results into a set of partial differential equations of parabolic type for the temperature distribution and of elliptic type for the radiative field. The main advantage of these simplified mathematical models lies in the fact that the governing equations are independent of the directional coordinates and easy to numerically solve using well established computational tools. In addition, under the assumption that the medium is optically thick, the derived approximations asymptotically recover the full radiative heat transfer in phase-change for the leading order. To solve the coupled nonlinear equations for radiative heat transfer in phase-change media, we have implemented a mixed finite element method for the space discretization along with a second-order implicit scheme for the time integration. The resulting nonlinear systems of algebraic equations have been dealt with using a Newton-based algorithm.

To examine the performance of the proposed simplified models we have solved several test problems for coupled radiative heat transfer and phase change in two- and three-dimensional enclosures including internal melting or solidification processes. Verification of the asymptotic analysis has also been carried out by comparing the results obtained using the simplified P_N approximations to those obtained using the full radiative transfer model for different optical scales. For the considered problems under the selected radiation conditions, it has been observed that radiative effects alter both the temperature distributions and the phase-change interfaces during the solidification and melting processes. It has been found that using these simplified models, it is possible to account for radiation in phase-change problems with a computational cost very significantly lower than solving the intro-differential equations for radiative heat transfer. It should be stressed that although we have restricted our study to coupled radiative heat transfer and phase-change problems in grey media, the proposed techniques can also be extended to model radiative heat transfer in non-grey absorbing and emitting media under phase change. For non-grey media and enclosures with high spatial dimensions, the full radiative transfer equations become even more complicated, requiring consideration of not only spatial and time variables but also frequency and directional variables. In this case, a multiband approach can be used to derive the simplified P_N approximations for the radiative transfer equation. However, the additional difficulties that arise when coupled with phase-change problems would be on developing a consistent approach to account for the variation of the optical spectrum when the material changes from one phase to another. This will be the addressed in a future work. Moreover, in many practical applications of radiative heat transfer in phase-change media, the medium is heterogeneous and not isotropic for which the involved parameters are required to depend on the space and direction coordinates. These and further issues are also subject of future investigations. Future work will also focus on extending these models to solve radiation-convection in phase-change media.

CRediT authorship contribution statement

Youssef Belhamadia: Writing – review & editing, Writing – original draft, Visualization, Validation, Software, Methodology, Funding acquisition, Conceptualization. **Mohammed Seaid:** Writing – review & editing, Writing – original draft, Methodology, Funding acquisition, Conceptualization.

Declaration of competing interest

The authors declare that they have no known competing financial interests or personal relationships that could have appeared to influence the work reported in this paper.

Acknowledgement

The authors wish to acknowledge the financial support provided by the Royal Society under the contract IES-R2-202078 and the financial support provided by the American University of Sharjah through the FRG grant. The work in this paper was supported, in part, by the Open Access Program from the American University of Sharjah. This paper represents the opinions of the author(s) and does not mean to represent the position or opinions of the American University of Sharjah.

Appendix A. Boundary conditions for the radiative intensity

On the boundary, the radiative intensity satisfies the following conditions

$$\begin{cases} \psi(\hat{\boldsymbol{x}},\boldsymbol{s}) &= \varrho_s(\boldsymbol{n}\cdot\boldsymbol{s})\psi(\hat{\boldsymbol{x}},\boldsymbol{s}') + \Big(1-\varrho_s(\boldsymbol{n}\cdot\boldsymbol{s})\Big)B(T_b,n_b), & (\hat{\boldsymbol{x}},\boldsymbol{s})\in\partial\Omega_s^-\cap\partial\Omega\times\mathbb{S}^2,\\ \psi(\hat{\boldsymbol{x}},\boldsymbol{s}) &= \varrho_l(\boldsymbol{n}\cdot\boldsymbol{s})\psi(\hat{\boldsymbol{x}},\boldsymbol{s}') + \Big(1-\varrho_l(\boldsymbol{n}\cdot\boldsymbol{s})\Big)B(T_b,n_b), & (\hat{\boldsymbol{x}},\boldsymbol{s})\in\partial\Omega_l^-\cap\partial\Omega\times\mathbb{S}^2, \end{cases} \tag{A.1}$$

where $\boldsymbol{s}' = \boldsymbol{s} - 2(\boldsymbol{n}\cdot\boldsymbol{s})\boldsymbol{n}$ is the specular reflection of $\boldsymbol{s}$ on $\partial\Omega$, and ϱ_k is the reflectivity coefficient of the phase k defined according to the Fresnel and Snell laws [52]. Therefore, for an incident angle θ_k given by $\cos\theta_k = |\mathbf{n}\cdot\boldsymbol{s}|$ and the Snell law

$$n_b\sin\theta_b = n_k\sin\theta_k,$$

the reflectivity $\varrho_k(\mu)$ with $\mu = |\boldsymbol{n}\cdot\boldsymbol{s}|$ is defined as follows

$$\varrho_k(\mu) = \begin{cases} \dfrac{1}{2}\left(\dfrac{\tan^2(\theta_k-\theta_b)}{\tan^2(\theta_k+\theta_b)} + \dfrac{\sin^2(\theta_k-\theta_b)}{\sin^2(\theta_k+\theta_b)}\right), & \text{if} \quad \Big|\sin\theta_k\Big| \le \dfrac{n_b}{n_k},\\ 1, & \text{otherwise}, \end{cases} \tag{A.2}$$

where $n_b < n_k$ is the refractive index of the surrounding medium and the hemispheric emissivity α_k is related to the reflectivity ϱ_k by

$$\alpha_k = 2n_k\int_0^1\Big(1-\varrho_k(\mu)\Big)\,d\mu.$$

In (A.1), the boundary region $\partial\Omega_k^-$ is defined as

$$\partial\Omega_k^- = \Big\{\hat{\boldsymbol{x}}\in\partial\Omega_k:\quad \boldsymbol{n}(\hat{\boldsymbol{x}})\cdot\boldsymbol{s}<0\Big\},\qquad k=s,l.$$

Appendix B. Parameters for boundary conditions in SP_N equations

In this appendix, we briefly summarize the variables required in the boundary conditions for the coupled SP_1-phase change equations (20)-(21) and coupled SP_3-phase change equations (22)-(23) and for a detailed derivation of these conditions we refer the reader to [37]. Hence, define the integrals R_i, $i = 1,2,\ldots,7$ by

$$R_1 = \int_0^1 \mu\varrho(-\mu)d\mu,\qquad R_2 = \int_0^1 \mu^2\varrho(-\mu)d\mu,\qquad R_3 = \int_0^1 \mu^3\varrho(-\mu)d\mu,\qquad R_4 = \int_0^1 \mu\mathcal{P}_3(\mu)\varrho(-\mu)d\mu,$$

$$R_5 = \int_0^1 \mathcal{P}_3(\mu)\varrho(-\mu)d\mu,\qquad R_6 = \int_0^1 P_1(\mu)\mathcal{P}_3(\mu)\varrho(-\mu)d\mu,\qquad R_7 = \int_0^1 P_3(\mu)\mathcal{P}_3(\mu)\varrho(-\mu)d\mu,$$

where ϱ is the reflectivity function given by (A.2), $\mathcal{P}_1$ and $\mathcal{P}_3$ are Legendre polynomials of order 1 and 3 defined as

$$\mathcal{P}_1(\mu) = \mu,\qquad \mathcal{P}_3(\mu) = \frac{5}{2}\mu^3 - \frac{3}{2}\mu.$$

Hence, the parameter ζ required in (21) for boundary conditions of the coupled SP_1-phase change equations is given by

$$\zeta = \frac{2+3R_2}{1-2R_1}.$$

The constants appeared in (23) for boundary conditions of the coupled SP_3-phase change equations (22)-(23) are summarized as

$$\mu_1^2 = \frac{1}{7}\left(3-2\sqrt{\frac{6}{5}}\right),\qquad \gamma_1 = \frac{5}{7}\left(1-3\sqrt{\frac{6}{5}}\right),$$

$$\mu_2^2 = \frac{1}{7}\left(3+2\sqrt{\frac{6}{5}}\right),\qquad \gamma_2 = \frac{5}{7}\left(1+3\sqrt{\frac{6}{5}}\right),$$

$$\varpi_1 = \frac{C_1D_4 - C_4D_1}{C_3D_4 - D_3C_4},\qquad \beta_1 = \frac{C_3D_1 - C_1D_3}{C_3D_4 - D_3C_4},\qquad \eta_1 = \frac{D_4\rho_1 - C_4\rho_3}{C_3D_4 - D_3C_4},$$

$$\varpi_2 = \frac{C_3D_2 - C_2D_3}{C_3D_4 - D_3C_4},\qquad \beta_2 = \frac{C_2D_4 - C_4D_2}{C_3D_4 - D_3C_4},\qquad \eta_2 = \frac{C_3\rho_3 - D_3\rho_1}{C_3D_4 - D_3C_4},$$

where

$$A_1 = \frac{1-2R_1}{4}, \qquad B_1 = -\frac{1+8R_5}{16}, \qquad C_1 = w_0(\gamma_2 A_1 - A_2), \qquad D_1 = w_0(\gamma_2 B_1 - B_2),$$
$$A_2 = \frac{5(1-8R_3)}{16}, \qquad B_2 = \frac{5(1-8R_6)}{16}, \qquad C_2 = w_0(-\gamma_1 A_1 + A_2), \qquad D_2 = w_0(-\gamma_1 B_1 + B_2),$$
$$A_3 = \frac{1+3R_2}{6}, \qquad B_3 = \frac{3R_4}{6}, \qquad C_3 = w_0(\gamma_2 A_3 - A_4), \qquad D_3 = w_0(\gamma_2 B_3 - B_4),$$
$$A_4 = R_4 + \frac{2}{9}(1+3R_2), \qquad B_4 = R_4 + \frac{3}{14}(1+7R_7), \qquad C_4 = w_0(-\gamma_1 A_3 - A_4), \qquad D_4 = w_0(-\gamma_1 B_3 + B_4),$$

with $w_0 = \frac{7}{36}\sqrt{\frac{6}{5}}$, ρ_1 and ρ_3 are given by

$$\rho_1 = \left(1-2R_1\right)\pi \qquad \text{and} \qquad \rho_3 = -\left(\frac{1}{4}+2R_5\right)\pi.$$

To approximate the one-dimensional integrals R_i, $i = 1, 2, \ldots, 7$, we use the Gauss-Legendre quadrature. It should be noted that the above parameters depend only on the optical reflectivity of the material where the radiation needs to be estimated and therefore, they can be calculated in advance and stored to be used during the simulation process. It is also evident that for non-reflective materials ($\varrho = 0$) these variables reduce to simple constants obtained by setting $R_i = 0$, for $i = 1, 2, \ldots, 7$ in the above equations.

Data availability

The data that support the findings of this study are available from the corresponding author upon reasonable request.

References

[1] S. Zhang, Y. Yao, Y. Jin, Z. Shang, Y. Yan, Heat transfer characteristics of ceramic foam/molten salt composite phase change material (CPCM) for medium-temperature thermal energy storage, Int. J. Heat Mass Transf. 196 (2022) 123262.
[2] M. Belaed, M. Rahman, R. Guldiken, Influence of optical thickness on the melting of a phase change material in a thermal energy storage module, JOM: J. Miner. Met. Mater. Soc. 72 (2020) 2089–2095.
[3] M. Ghalambaz, M. Aljaghtham, A.J. Chamkha, A. Abdullah, I. Mansir, M. Ghalambaz, Mathematical modeling of heterogeneous metal foams for phase-change heat transfer enhancement of latent heat thermal energy storage units, Appl. Math. Model. 115 (2023) 398–413.
[4] S. Mitchell, M. Vynnycky, Verified reduction of a model for a continuous casting process, Appl. Math. Model. 48 (2017) 476–490.
[5] Y. Belhamadia, G.O. Cassol, S. Dubljevic, Numerical modelling of hyperbolic phase change problems: application to continuous casting, Int. J. Heat Mass Transf. 209 (2023) 124042.
[6] A. Bar-Cohen, Encyclopedia of Thermal Packaging, Set 1: Thermal Packaging Techniques (a 6-Volume Set), World Scientific, 2012.
[7] M. Abrams, R. Viskanta, The effects of radiative heat transfer upon the melting and solidification of semitransparent crystals, ASME J. Heat Mass Transf. 96 (2) (May 1974) 184–190.
[8] R. Viskanta, E. Anderson, Heat transfer in semitransparent solids, Adv. Heat Transf. 11 (1975) 317–441.
[9] D. Mihalas, B. Mihalas, Foundations of Radiation Hydrodynamics, Oxford University Press, New York, 1983.
[10] E. Lewis, W. Miller, Computational Methods of Neutron Transport, John Wiley & Sons, New York, 1984.
[11] C.-H. Wang, Y.-Y. Feng, K. Yue, X.-X. Zhang, Discontinuous finite element method for combined radiation-conduction heat transfer in participating media, Int. Commun. Heat Mass Transf. 108 (2019) 104287.
[12] Y.-Y. Feng, C.-H. Wang, Discontinuous finite element method applied to transient pure and coupled radiative heat transfer, Int. Commun. Heat Mass Transf. 122 (2021) 105156.
[13] C.-H. Wang, X.-Y. Zhang, C.-C. Pan, Z.-Y. Jiang, Unified discontinuous Galerkin finite-element framework for transient conjugated radiation-conduction heat transfer, Phys. Rev. E 107 (4) (2023) 045303.
[14] Y. Belhamadia, M. Seaid, Computing enhancement of the nonlinear SP_N approximations of radiative heat transfer in participating material, J. Comput. Appl. Math. 434 (2023) 115342.
[15] H. Fang, Q. Zhang, J. Tian, S. Wang, R. Ma, Study of internal radiation with solute inclusions during Czochralski sapphire crystal growth, Int. J. Heat Mass Transf. 79 (2014) 783–789.
[16] P. Lapka, P. Furmański, Fixed grid simulation of radiation-conduction dominated solidification process, ASME J. Heat Mass Transf. 132 (2) (February 2010) 023504.
[17] P. Łapka, P. Furmański, Numerical modelling of solidification processes of semitransparent materials using the enthalpy and the finite volume methods, Heat Mass Transf. 44 (2008) 937–957.
[18] C. Jing, A. Hayashi, M. Kobayashi, T. Tsukada, M. Hozawa, N. Imaishi, K. Shimamura, N. Ichinose, Effect of internal radiative heat transfer on spoke pattern on oxide melt surface in Czochralski crystal growth, J. Cryst. Growth 259 (4) (2003) 367–373.
[19] A. Maroufi, C. Aghanajafi, Analysis of conduction–radiation heat transfer during phase change process of semitransparent materials using lattice Boltzmann method, J. Quant. Spectrosc. Radiat. Transf. 116 (2013) 145–155.
[20] Rishi Raj, Amit Prasad, Pritish Ranjan Parida, Subhash C. Mishra, Analysis of solidification of a semitransparent planar layer using the lattice Boltzmann method and the discrete transfer method, Numer. Heat Transf., Part A, Appl. 49 (3) (2006) 279–299.
[21] S.C. Mishra, N.C. Behera, A.K. Garg, A. Mishra, Solidification of a 2-d semitransparent medium using the lattice Boltzmann method and the finite volume method, Int. J. Heat Mass Transf. 51 (17) (2008) 4447–4460.
[22] C. Yao, B. Chung, G.-X. Wang, Mushy zone equilibrium solidification of a semitransparent layer subject to radiative and convective cooling, Int. J. Heat Mass Transf. 45 (11) (2002) 2397–2405.
[23] H.-L. Yi, H.-P. Tan, Y. Zhou, Coupled radiation and solidification heat transfer inside a graded index medium by finite element method, Int. J. Heat Mass Transf. 54 (13) (2011) 3090–3095.
[24] M. Kumar, S. Roy, S.S. Panda, Numerical simulation of continuous casting of steel alloy for different cooling ambiences and casting speeds using immersed boundary method, Proc. Inst. Mech. Eng., B J. Eng. Manuf. 231 (8) (2017) 1363–1378.

[25] A.R. Archibold, M.M. Rahman, D. Yogi Goswami, E.K. Stefanakos, The effects of radiative heat transfer during the melting process of a high temperature phase change material confined in a spherical shell, Appl. Energy 138 (2015) 675–684.
[26] M. Modest, J. Yang, Elliptic pde formulation and boundary conditions of the spherical harmonics method of arbitrary order for general three-dimensional geometries, J. Quant. Spectrosc. Radiat. Transf. 109 (9) (2008) 1641–1666.
[27] E. Gelbard, Simplified spherical harmonics equations and their use in shielding problems, Technical Report WAPD-T-1182, Bettis Atomic Power Laboratory, 1961.
[28] S. Rosseland, Theoretical Astrophysics: Atomic Theory and the Analysis of Stellar Atmospheres and Envelopes, Clarendon Press, Oxford, 1936.
[29] M. Frank, M. Seaid, J. Janicka, A. Klar, R. Pinnau, G. Thömmes, A comparison of approximate models for radiation in gas turbines, Prog. Comput. Fluid Dyn. 3 (2004) 191–197.
[30] A. Klar, J. Lang, M. Seaid, Adaptive solutions of SP_N-approximations to radiative heat transfer in glass, Int. J. Therm. Sci. 44 (2005) 1013–1023.
[31] R. Backofen, T. Bilz, A. Ribalta, A. Voigt, SP_N-approximations of internal radiation in crystal growth of optical materials, J. Cryst. Growth 266 (2004) 264–270.
[32] M. Seaid, M. Frank, A. Klar, R. Pinnau, G. Thömmes, Efficient numerical methods for radiation in gas turbines, J. Comput. Appl. Math. 170 (2004) 217–239.
[33] M. Frank, A. Klar, E. Larsen, S. Yasuda, Approximate models for radiative transfer, Bull. Inst. Math. Acad. Sin. 2 (2) (2007) 409.
[34] M. Seaid, A. Klar, R. Pinnau, Numerical solvers for radiation and conduction in high temperature gas flows, Flow Turbul. Combust. 75 (2005) 173–190.
[35] X.-Y. Zhang, C.-H. Wang, Development and application of discontinuous Galerkin method for solidification problems in a semitransparent medium-filled cavity, J. Energy Storage 71 (2023) 108023.
[36] F.-E. Moutahir, Y. Belhamadia, M. Seaid, M. El-Amrani, Modelling and simulation of radiative heat transfer in non-grey absorbing and emitting media under phase change, Comput. Math. Appl. 176 (2024) 432–446.
[37] E. Larsen, G. Thömmes, A. Klar, M. Seaid, T. Götz, Simplified P_N approximations to the equations of radiative heat transfer and applications, J. Comput. Phys. 183 (2002) 652–675.
[38] Y. Belhamadia, M. Seaid, A mixed finite element method for nonlinear radiation–conduction equations in optically thick anisotropic media, Math. Comput. Simul. 216 (2024) 15–29.
[39] Y. Belhamadia, Modélisation mathématique et simulation numérique de problèmes de changement de phase avec applications à la cryochirurgie, Ph.D. thesis, Université Laval, 2004.
[40] H. Yao, M. Azaiez, A monolithic model of solid–liquid phase change problem, Comput. Methods Appl. Mech. Eng. 421 (2024) 116794.
[41] Y. Belhamadia, A. Fortin, É. Chamberland, Anisotropic mesh adaptation for the solution of the Stefan problem, J. Comput. Phys. 194 (1) (2004) 233–255.
[42] Y. Belhamadia, A. Fortin, É. Chamberland, Three-dimensional anisotropic mesh adaptation for phase change problems, J. Comput. Phys. 201 (2) (2004) 753–770.
[43] A. Fortin, Y. Belhamadia, Numerical prediction of freezing fronts in cryosurgery: comparison with experimental results, Comput. Methods Biomech. Biomed. Eng. 8 (4) (2005) 241–249.
[44] M. Modest, Radiative Heat Transfer, McGraw-Hill, 1993.
[45] S. Giani, M. Seaid, hp-adaptive discontinuous Galerkin methods for simplified P_N approximations of frequency-dependent radiative transfer, Comput. Methods Appl. Mech. Eng. 301 (2016) 52–79.
[46] Jaafar Albadr, Mofdi El-Amrani, Mohammed Seaid, Simplified P_N finite element approximations for coupled natural convection and radiation heat transfer, Numer. Heat Transf., Part A, Appl. 83 (5) (2023) 478–502.
[47] Y. Belhamadia, A. Fortin, T. Briffard, A two-dimensional adaptive remeshing method for solving melting and solidification problems with convection, Numer. Heat Transf., Part A, Appl. 76 (4) (2019) 179–197.
[48] S. Balay, K. Buschelman, V. Eijkhout, W. Gropp, D. Kaushik, M. Knepley, L.C. McInnes, B. Smith, H. Zhang, PETSc Users Manual, Tech. Rep. ANL-95/11-Revision 2.1.6, Argonne National Laboratory, Argonne, Illinois, 2003.
[49] Y. Saad, Iterative Methods for Sparse Linear Systems, PWS Publishing Company, 1996.
[50] M. Seaid, A. Klar, Efficient preconditioning of linear systems arising from the discretization of radiative transfer equation, Lect. Notes Comput. Sci. 35 (2003) 211–236.
[51] L. Begum, M. Hasan, 3-d prediction of alloy solidification in the presence of turbulent flow in a vertical direct chill caster with a porous filter near the top, Appl. Math. Model. 40 (21) (2016) 9029–9051.
[52] R. Viskanta, Radiative Transfer in Combustion Systems: Fundamental and Applications, Begell House Publishers, 2005.